HHS Public Access

Author manuscript

Immunity. Author manuscript; available in PMC 2022 March 09.

Published in final edited form as:

Immunity. 2021 March 09; 54(3): 484–498.e8. doi:10.1016/j.immuni.2021.01.004.

Dectin-1 limits autoimmune neuroinflammation and promotes myeloid cell-astrocyte crosstalk via Card9-independent expression of Oncostatin M

M. Elizabeth Deerhake[1], **Keiko Danzaki**[1], **Makoto Inoue**[1,2], **Emre D. Cardakli**[1], **Toshiaki Nonaka**[1], **Nupur Aggarwal**[1], **William E. Barclay**[1], **Ru-Rong Ji**[3], **Mari L. Shinohara**[1,4,*]

[1]Department of Immunology, Duke University School of Medicine, Durham, NC 27710, USA.

[2]Department of Comparative Biosciences, University of Illinois at Urbana-Champaign, Urbana, IL 61820, USA.

[3]Department of Anesthesiology, Duke University School of Medicine, Durham, NC 27710, USA.

[4]Department of Molecular Genetics and Microbiology, Duke University School of Medicine, Durham, NC 27710, USA.

SUMMARY

Pathologic roles for innate immunity in neurologic disorders are well-described, but their beneficial aspects are less understood. Dectin-1, a C-type lectin receptor (CLR), is largely known to induce inflammation. Here we report that Dectin-1 limited experimental autoimmune encephalomyelitis (EAE), while its downstream signaling molecule, Card9, promoted the disease. Myeloid cells mediated the pro-resolution function of Dectin-1 in EAE with enhanced gene expression of the neuroprotective molecule, Oncostatin M (Osm), through a Card9-independent pathway, mediated by the transcription factor NFAT. Furthermore, we found that the Osm receptor (OsmR) functioned specifically in astrocytes to reduce EAE severity. Notably, Dectin-1 did not respond to heat-killed *Mycobacteria*, an adjuvant to induce EAE. Instead, endogenous Dectin-1 ligands, including galectin-9, in the central nervous system (CNS) were involved to limit EAE. Our study reveals a mechanism of beneficial myeloid cell-astrocyte crosstalk regulated by a Dectin-1 pathway and identifies potential therapeutic targets for autoimmune neuroinflammation.

Graphical Abstract

[*]**Lead Contact:** Mari Shinohara, mari.shinohara@duke.edu.

AUTHOR CONTRIBUTIONS

MED, KD, MI, and MLS designed experiments, analyzed and interpreted data. MED performed experiments apart from the following contributions: KD and MI performed experiments in Fig. 1A–B; D–F and Fig. S1D, E, G, H. KD performed experiments in Fig. 7B, C and Fig. S7A. TN assisted with experiments in Fig. 6A–F. EC assisted with experiments in Fig. S5B, D; Fig. 7F; Fig. S7E. NA assisted with experiments in Fig. 1C. WB provided assistance with EAE methods and experiment design. RRJ provided support with RNAscope *in situ* hybridization. MED and MLS wrote the manuscript with editing by the other co-authors.

DECLARATION OF INTERESTS

Ru-Rong Ji is a consultant of Boston Scientific and received research grant from the company. This activity is not related to the current study. The remaining authors declare no competing interests.

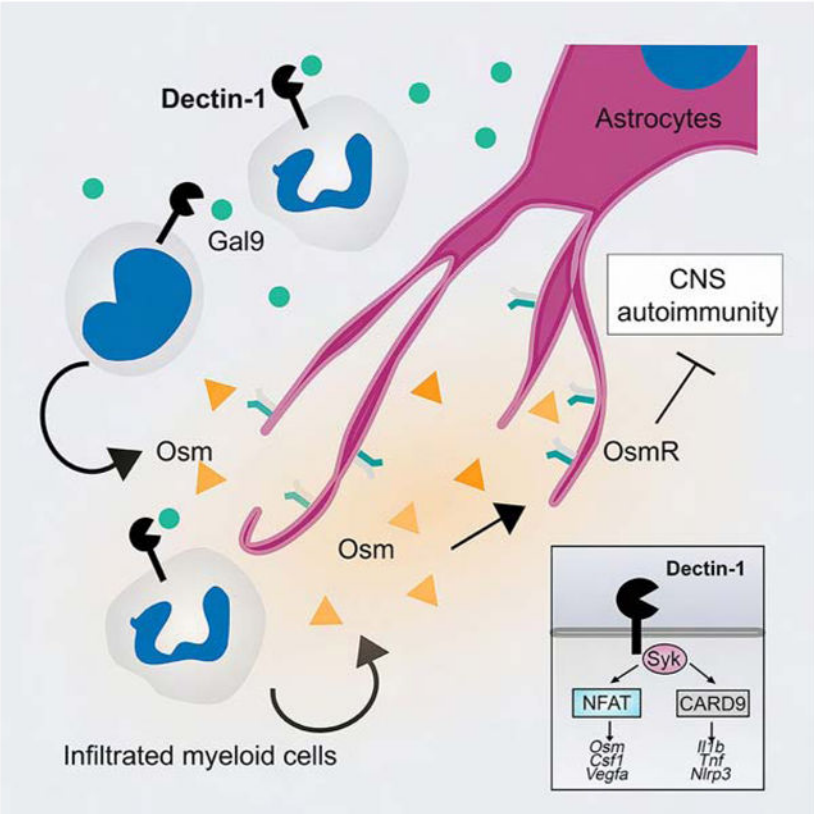

eTOC BLURB

Pattern recognition receptor signaling can regulate neuroinflammation in animal model of Multiple Sclerosis (MS). Deerhake et al. now show that Dectin-1 promotes beneficial myeloid cell-astrocyte cross talk in EAE by upregulating Oncostatin M through a Card9-independent pathway.

INTRODUCTION

The innate immune response contributes to both damage and repair in central nervous system (CNS) autoimmunity, and pattern recognition receptors (PRRs) are key to orchestrating innate immune responses (Deerhake et al., 2019; Dendrou et al., 2015). Among PRRs, the C-type lectin receptor (CLR) family, including Dectin-1, has been studied mainly in fungal infections and remains less characterized in sterile inflammation and autoimmune disorders, including multiple sclerosis (MS) (Deerhake et al., 2019). Dectin-1 induces interleukin-1β (IL-1β) and resulting T helper-17 (Th17) cell responses during fungal infections via Card9/− and NFκB signaling (Gross et al., 2006; LeibundGut-Landmann et al., 2007). Although Dectin-1 is known as a receptor for fungal β-glucans (Taylor et al., 2007), some studies have identified host-derived endogenous ligands for Dectin-1, as well as functions of Dectin-1 signaling beyond the setting of fungal infections (Bode et al., 2019; Daley et al., 2017; Roesner et al., 2019; Shan et al., 2013; Thiagarajan et al., 2013). Notably, in one (Stoppelkamp et al., 2015) of three reports (Brown et al., 2017; Lee et al., 2016) of

experimental autoimmune uveitis (EAU), Dectin-1 has been found to be detrimental. Dectin-1 also appears to be pathogenic in animal models of spinal cord injury (Gensel et al., 2015) and stroke (Ye et al., 2020). Nevertheless, the function of Dectin-1 in CNS disorders may depend on the type of neuropathology, and the role of Dectin-1 in autoimmunity and neuroinflammation is still largely unexplored.

Given the well-described pro-inflammatory functions of Dectin-1 signaling, one may predict that Dectin-1 would exacerbate neuroinflammation in the EAE model of multiple sclerosis (MS). However, the present study demonstrates that Dectin-1 signaling in myeloid cells limits neuroinflammation and EAE severity, although a major Dectin-1 signaling molecule, Card9, promotes disease development. We found that Card9-independent Dectin-1 signaling involving the transcription factor NFAT, drove expression of Oncostatin M (Osm), an IL-6 family cytokine with neuroprotective functions (Janssens et al., 2015; Slaets et al., 2014; Wallace et al., 1999), and signaling through the Osm receptor (OsmR) on astrocytes reduced disease progression and promoted recovery in EAE. Furthermore, we identified a Card9-independent Dectin-1-mediated transcriptional program driving expression of *Osm* and other neuroprotective genes. Our findings provoke a re-consideration of Dectin-1 signaling and functions by identifying a mechanism of beneficial myeloid cell-astrocyte communication in CNS autoimmunity.

RESULTS

Elevated gene expression of the C-type lectin receptor, Dectin-1 (*CLEC7A*) are evident in MS lesions

We evaluated gene expression of CLRs in multiple datasets profiling MS brain lesions (GSE10800, GSE123496). Among genes encoding CLRs with known immune functions, *CLEC7A* (Dectin-1) and *CLEC4A* (DCIR) were notable for their elevated expression in MS brain specimens in two independent datasets (Fig. S1A–C)(Hendrickx et al., 2017; Voskuhl et al., 2019), suggesting possible involvement of Dectin-1 and DCIR in MS. In EAE, DCIR has been reported to be protective (Seno et al., 2015; Uto et al., 2016) but the function of Dectin-1 in autoimmune neuroinflammation remains unknown.

Dectin-1 is a beneficial C-type lectin receptor in EAE

Next, we sought to test the function of Dectin-1 in CNS autoimmunity using EAE induced with the $MOG_{35–55}$ autoantigen peptide. We initially hypothesized that Dectin-1 may exacerbate EAE severity by promoting IL-1β expression and Th17 cell differentiation, given its known role in antifungal immunity (Gross et al., 2006; LeibundGut-Landmann et al., 2007) and the pathogenicity of Th17 cells in EAE development. Instead, we found that Dectin-1-deficient (*Clec7a*$^{-/-}$) mice developed more severe disease than WT mice (Fig. 1A). A mild EAE induction with a reduced amount of adjuvant also showed the beneficial effect of Dectin-1 (Fig. 1B). Next, we tested whether administering a Dectin-1 agonist was sufficient to limit EAE severity. To test this, we used hot alkali-depleted zymosan (d-zymosan), which is specific to Dectin-1 but does not stimulate Toll-like receptor-2 (TLR2) (Ikeda et al., 2008). d-zymosan has an advantage over curdlan, another Dectin-1-specific ligand, for safe intravenous (*i.v.*) use in EAE possibly due to zymosan's smaller particle

size. We did not observe complication by injecting d-zymosan, although a majority of mice died by curdlan *i.v.* injection (*unpublished data*). Indeed, a single *i.v.* injection of d-zymosan on one day post-immunization (dpi) inhibited EAE development (Fig. 1C). Together, these results indicate that Dectin-1 limits EAE severity.

Dectin-1 limits CNS inflammation in EAE

To determine how Dectin-1 regulates EAE, we evaluated immune cell subsets by flow cytometry in secondary lymphoid organs and in the spinal cord (SC) of WT and *Clec7a*$^{-/-}$ mice. Both groups showed no significant difference in numbers of various cell types in spleen and lymph node (LN) at 9-dpi (Fig. S1D–I). Additionally, no major effect on CD4^{+} T cell phenotypes by Dectin-1 was suggested based on numbers of regulatory T (Treg), Th1, Th17, or granulocyte macrophage colony stimulating factor (GM-CSF)$^{+}$ Th cells, MOG recall responses, and IL-10 production by CD25^{+}CD4^{+} T cells (Fig. 1D, Fig. S1J–L). Similarly, d-zymosan did not impact total cell numbers and the cellularity of various T helper cells, myeloid cell numbers, and *ex vivo* T cell recall response (Fig S2A–F). In summary, we did not observe substantial effects of Dectin-1 on the peripheral immune response that would explain the elevated disease severity in *Clec7a*$^{-/-}$ mice.

In contrast to the phenotype in the periphery, *Clec7a*$^{-/-}$ mice had elevated immune cell infiltration in the SC at 9-dpi across multiple immune cell subsets (Fig. 1E, F), suggesting that Dectin-1 broadly limited inflammation in the SC during EAE. Notably, CNS myeloid cells from *Clec7a*$^{-/-}$ mice did not show elevated surface expression of CD40, CD80, or CD86, suggesting no major alteration in myeloid cell activation (Fig. S2G). We also observed increased demyelination in SCs of *Clec7a*$^{-/-}$ mice by Luxol fast blue/periodic acid-Schiff (LFB-PAS) staining (Fig. 1G; Fig. S2H). Together, this demonstrates that Dectin-1 limits CNS inflammation during EAE.

To test whether Dectin-1 reduces immune cell migration to the CNS in a cell-intrinsic manner, we generated mixed bone-marrow (BM) chimeras reconstituted with both WT and *Clec7a*$^{-/-}$ BM cells (Fig. S2I, J). Following EAE induction, the relative proportion of CD11b^{+} myeloid cells derived from WT and *Clec7a*$^{-/-}$ BM cells were comparable in the spleen and the SC (Fig. S2K), suggesting Dectin-1 does not limit myeloid cell infiltration into the CNS in a cell-intrinsic manner. In summary, Dectin-1 decreased neuroinflammation in EAE, but this effect was not attributable to altered T helper cell polarization, CNS myeloid cell activation, or cell-intrinsic defects in myeloid cell migration into the CNS.

Card9 exacerbates EAE and promotes Th17 cell responses

Next, we evaluated the role of Card9, a major mediator of Dectin-1 signaling, in EAE. As expected, *Card9*$^{-/-}$ mice developed alleviated disease than WT controls (Fig. 2A), indicating that Card9, unlike Dectin-1, is pathogenic in EAE. Next, we used a BM chimera system to test whether immune cells were sufficient to mediate Card9 function in EAE. Indeed, recipients reconstituted with *Card9*$^{-/-}$ BM cells were resistant to EAE development, indicating that BM-derived immune cells are responsible for Card9 function (Fig. 2B).

Not only did Card9 and Dectin-1 show divergent functions in EAE, the immune cell profile of *Card9*$^{-/-}$ mice in EAE was also clearly distinct from that of *Clec7a*$^{-/-}$ mice, particularly

regarding T cell phenotypes. In *Card9*$^{-/-}$ mice, numbers of IL-17^{+}IFNγ^{+} Th cells were reduced in inguinal lymph nodes (ILNs) and CD25^{+}CD4^{+} T cells had enhanced ability to produce IL-10 *ex vivo*, while no differences were found in Treg $_{cell}$ numbers and T cell recall responses difference (Fig. 2 C–E; Fig. S3A–D). Numbers of neutrophils were also reduced in *Card9*$^{-/-}$ mice in the spleen (Fig. 2F). Although numbers of other individual cell types did not reach statistical significance, total cell numbers were reduced in the periphery of *Card9*$^{-/-}$ mice at 9-dpi (Fig. 2F, G; Fig. S3E–G). In summary, although Dectin-1 limits EAE, Card9 is pathogenic particularly with an enhanced encephalitogenic T cells and neutrophils.

Peripheral and CNS-resident myeloid cells express Dectin-1 in EAE

We next evaluated Dectin-1 expression under naïve and EAE conditions. Dectin-1 was expressed on neutrophils, monocytes, macrophages, and DCs in the spleen under naïve and EAE conditions, but not on T and B cells (Fig. 3A; Fig. S4A). During EAE, neutrophils and monocytes were the predominant Dectin-1-expressing cell types in the spleen (Fig. 3B). In the SC of EAE mice, Dectin-1^{+} cells were identified in white matter and co-localized with CD11b antibody staining signal, indicative of myeloid cells (Fig. 3C). Particularly for Iba1^{+} cells, Dectin-1 expression was more intensive in Iba1^{+} cells with amoeboid morphology than those with ramified morphology (Fig. S4B). Immunofluorescent (IF) histology did not show Dectin-1 expression by Tmem119^{+} microglia (Fig. S4C), but flow-cytometry did detect upregulation of Dectin-1 expression in microglia (Tmem119^{+}CD11b^{lo}CD45^{lo}) during EAE (Fig. S4D; Fig. 3D). Nevertheless, CNS-infiltrated myeloid cells had higher Dectin-1 expression than microglia did even in EAE mice (Fig. 3D).

Cells of hematopoietic origin mediate Dectin-1 function in EAE

To evaluate the contribution of hematopoietic-derived cells, we used a BM chimera approach. Specifically, we generated BM chimeras by adoptively transferring BM cells from *Clec7a*$^{-/-}$ or WT donor mice to WT recipients (Fig. S4E) or by transferring BM cells from WT donor mice to *Clec7a*$^{-/-}$ or WT recipients. Chimeras that received *Clec7a*$^{-/-}$ BM cells exhibited more severe disease than chimeras which received WT BM cells (Fig. 3E). Without Dectin-1 expression by lymphoid cells (Fig. S4A), this result demonstrates that hematopoietic-derived myeloid cells are likely to mediate the effect of Dectin-1 in limiting EAE. In reciprocal experiments with WT BM cell transfer, no difference was found between *Clec7a*$^{-/-}$ and WT recipients (Fig. 3F), suggesting that radiation-resistant cells, including microglia, were less likely to mediate the negative regulatory function of Dectin-1. Although the irradiation BM chimera approach does not fully rule out the involvement of microglia (Larochelle et al., 2016), the results strongly suggest that hematopoietic-derived myeloid cells mediate the Dectin-1 function in EAE.

Dectin-1 promotes expression of neuroprotective cytokine, Oncostatin M (Osm)

Previous studies suggest that some CNS-infiltrating myeloid cells could have protective functions in CNS injury and repair (Gadani et al., 2015; Stirling et al., 2009). Thus, we wondered whether the beneficial role of Dectin-1 could be mediated by neuroprotective factors expressed by myeloid cells. To investigate this, we used splenic CD11b^{+} myeloid cells for initial examination with the Dectin-1-specific agonist, curdlan. Among the

candidate genes, encoding secreted proteins with neuroprotective functions, curdlan potently upregulated the expression of *Osm* (Fig. S4F), a multi-functional IL-6 family cytokine with neuroprotective roles in different CNS disorders (Guo et al., 2015; Houben et al., 2019; Janssens et al., 2015; Slaets et al., 2014). In addition to $CD11b^+$ splenocytes, primary neutrophils, monocytes, and BM-derived DCs (BMDCs) upregulated *Osm* expression (Fig. 4A, B). Upregulation of Osm protein by curdlan stimulation was confirmed in supernatants of neutrophil cell culture, as well as neutrophil cell lysates (Fig. S4G).

We next evaluated whether microglia could also upregulate *Osm* upon curdlan stimulation. Because of little Dectin-1 expression in microglia from naïve mice (Fig. 3D), we isolated Dectin-1-expressing microglia from EAE mice by flow-cytometry sorting $CD11b^{lo}CD45^{lo}$ cells, together with CNS-infiltrated myeloid cells ($CD11b^{hi}CD45^{hi}$), from WT EAE mice and stimulated them with curdlan. While CNS-infiltrated myeloid cells showed potent upregulation of *Osm*, microglia had a more muted response despite expressing Dectin-1 (Fig. 4 C, D). These results suggest that Dectin-1 signaling drives *Osm* expression in a cell-type-specific manner, whereby microglia show a more limited response than neutrophils, monocytes, and BM-derived dendritic cells (BMDC)s.

Osm expression is upregulated in the CNS during EAE

Osm protein expression is detected in MS lesions by histology (Ruprecht et al., 2001) and in culture supernatant of peripheral blood mononuclear cells (PBMCs) from MS patients (Ensoli et al., 2002). In EAE, we found an increase in serum Osm protein in WT EAE mice at 9-dpi, compared to WT naïve mice, while amounts of serum Osm protein in *Clec7a*$^{-/-}$ mice showed a slight but not statistically significant reduction at 9-dpi (Fig. S4J). Next, we sought to examine *in situ* Osm expression in the CNS during EAE. Because antibody (Ab) staining for Osm, a secreted cytokine, was diffuse and challenging to quantify in a cell-specific manner, we used RNAscope *in situ* mRNA hybridization to examine *Osm* expression in the CNS. SC from EAE mice at 17-dpi showed drastically increased *Osm* mRNA expression, observed particularly in ventral and lateral white matter lesions with corresponding DAPI-staining, reflecting peripheral cell infiltration (Fig. 4E, F). $CD11b^+$ cells are a substantial but not exclusive source of *Osm* mRNA in white matter lesions (Fig. 4G, S4K). *Clec7a*$^{-/-}$ mice with 17-dpi EAE had reduced *Osm* mRNA expression in $CD11b^+$ cells (Fig. 4H), although no significant difference was found in total SC homogenates (Fig. S4L). This suggests a local effect of Osm around myeloid cells, which are particularly responsible for Dectin-1-mediated *Osm* expression.

To determine which CNS myeloid cells express *Osm* during EAE at the single-cell level, we re-analyzed publicly available scRNAseq data from CNS myeloid cells in naïve and EAE conditions (GSE118948) (Fig. S4N, O). Neutrophils, monocytes, and microglia highly express both *Osm* and *Clec7a* during EAE (Fig. S4P, Q). Thus, we sought to confirm the results by PrimeFlow RNA assay, flow-cytometry based *in situ* hybridization. In *Clec7a*$^{-/-}$ mice, neutrophils showed a statistically significant reduction in *Osm* expression ($p<0.01$), while monocytes in *Clec7a*$^{-/-}$ mice showed a trend toward reduced *Osm* expression ($p=0.06$) (Fig. 4I, J). *Osm* expression by microglia and DCs were not altered between WT and *Clec7a*$^{-/-}$ mice (Fig. 4I). Based on these findings, we conclude that neutrophils and, to a

lesser extent, monocytes contribute to *Osm* expression induced by Dectin-1 in the CNS during EAE.

Card9-independent signaling promotes distinct Dectin-1 effector functions

Next, we investigated how *Osm* expression was enhanced by Dectin-1. Although Card9 is a critical signaling molecule downstream of Dectin-1, we found that Card9 was dispensable for *Osm* expression (Fig. 5A, Fig. S5A). Given the divergent functions for Card9 and Dectin-1 in EAE development (Fig. 1, 2), we hypothesize that Card9-independent signaling may activate a Dectin-1-mediated transcriptional program with distinct beneficial functions, as seen in driving *Osm* expression.

To further characterize the Card9-independent Dectin-1-mediated transcriptional program, we focused on neutrophils, because neutrophils are among the most abundant myeloid cells in the CNS during EAE (Caravagna et al., 2018), limit late-stage EAE (Knier et al., 2018), can be neuroprotective (Sas et al., 2020), and contribute to Dectin-1-dependent *Osm* expression in SC of EAE mice (Fig. 4I, J). RNA sequencing was performed with neutrophils treated with or without curdlan for 3-hrs. We first identified 1,157 genes which were upregulated or downregulated by Dectin-1 stimulation in WT neutrophils (Fig. 5B). Among those genes, 567 genes were regulated by a Card9-independent manner (Fig. 5C). Pathway analyses revealed that Card9-dependent genes showed enrichment in pathways for pro-inflammatory factors, such as TLR signaling, MyD88 signaling, and IL-1 signaling (Fig. 5D, E). In contrast, Card9-independent genes were enriched in pathways including iron uptake and processing, lysosome and Golgi vesicle biogenesis, glycolysis, cellular response to stress, and interleukin signaling (Fig. 5F, G). *Osm* was among the Card9-independent genes found in the interleukin signaling pathway, which includes both neuroprotective factors and negative regulators of pro-inflammatory signaling, such as an inhibitor of TLR signaling (*Tollip*), an inhibitor of NFκB signaling (*Nfkbib*), and the decoy receptor for IL-1 (*Il1r2*) (Fig. 5G). Other Card9-independent genes besides *Osm* with reported neuroprotective functions in EAE, include *Csf1* (Wlodarczyk et al., 2018), *Cd93* (Griffiths et al., 2018), and *Vegfa* (Stanojlovic et al., 2016) (Fig. 5G). The RNAseq results were confirmed by RT-qPCR (Fig. S5B). In addition to neutrophils, Card9-independent gene expression by Dectin-1 stimulation was confirmed in monocytes, macrophages, and DCs to an extent depending on cell-type (Fig. S5C, D). In summary, Card9-independent Dectin-1 signaling drives expression of *Osm* and other genes encoding neuroprotective molecules in multiple myeloid cell types.

NFAT mediates Card9-independent upregulation of *Osm* by Dectin-1

Next, we looked for enrichment of predicted transcription factor (TF)-binding sites near Dectin-1-regulated gene loci by focusing on open chromatin regions (OCRs) in BM neutrophils using publicly available ATAC-seq data from the Immunological Genome (ImmGen) Project. We first found that NFκB-family TF-binding sites were enriched in Card9-dependent genes but not in Card9-independent genes (Fig. 5H, I). In contrast, NFAT-family TF-binding sites were enriched in Card9-independent genes, and Card9-dependent genes showed some degree of enrichment (Fig. 5H, I). While we do not rule out the involvement of NFκB signaling in *Osm* regulation, no predicted NFκB-family TF binding

sites were identified in OCRs near *Osm* (Fig. 5J). Instead, OCRs in the *Osm* gene had multiple predicted NFAT-binding sites in both neutrophils and monocytes (Fig. S5E). Previous studies have shown that Dectin-1 can indeed induce NFAT activity through the Syk-PLCγ-Ca^{2+} signaling axis (Goodridge et al., 2007; Xu et al., 2009), but the transcriptional program downstream of this pathway remains less characterized compared to Card9 signaling.

Next, we used small molecule inhibitors to target signaling pathways downstream of Dectin-1 (Fig. 5K). Although inhibition of Raf1 did not block *Osm* upregulation by curdlan stimulation in neutrophils, inhibitors of Syk and NFAT did (Fig. 5L). Both inhibitors showed dose-dependent effects (Fig. 5L), and neither resulted in detectable cellular toxicity, suggesting that Dectin-1 enhances *Osm* expression via Syk and NFAT. Other genes, such as *Csf1* and *Vegfa*, behaved as *Osm* did, but some Card9-independent genes, such as *Cd93*, did not require NFAT for upregulation (Fig. S5F). Furthermore, interfering with NFAT signaling by inhibiting phospholipase C (PLC) and calcineurin (CaN) blocked *Osm* upregulation (Fig. 5M, N), indicating that CaN and PLC are involved. Reciprocally, ionomycin upregulated *Osm* expression even in the absence of curdlan stimulation (Fig. 5O), suggesting increased intracellular calcium is sufficient for *Osm* upregulation. These findings demonstrate that Dectin-1 signaling induces *Osm* expression through a Card9-independent pathway, which includes Syk, PLC, Ca^{2+}, CaN, and NFAT.

OsmR expressed on astrocyte limits EAE severity

Next, we sought to identify which cell types express OsmR. Astrocytes ($GFAP^+$, $ALDHL1L\text{-}eGFP^+$), and neurons ($Neurofilament^+$) to a lesser extent, in SC white matter expressed OsmR under naïve and EAE conditions (Fig. 6A–C; Fig. S6A, B). In contrast, we could not detect OsmR on oligodendrocytes, microglia, or $CD45^+$ immune cells (Fig. 6D–F). Furthermore, re-analysis of a published dataset (GSE100330) confirmed that *Osmr* expression is enriched in astrocytes compared to total CNS tissue in EAE SC (Fig S6C, D). Thus, while other CNS cell types have been reported to express OsmR (endothelial cells, microglia, neurons, oligodendrocytes), we focused our investigation on OsmR function in astrocytes given their high expression of *Osmr* mRNA (Fig. S6C) and protein (Fig. 6A, B). $Osmr^{fl/fl}$ mice were cryorecovered, backcrossed to the B6 background by a speed congenic approach, and crossed to generate $Gfap^{cre};Osmr^{fl/fl}$ mice with confirmed cre recombination (Fig. S6E–H). The $Gfap^{cre};Osmr^{fl/fl}$ mice had exacerbated disease severity compared to littermate controls ($Osmr^{fl/fl}$), particularly showing impaired remission (day 18–35)(Fig. 6G, H). OsmR deletion in astrocytes had no impact on leukocyte numbers in the periphery at 9-dpi and in the CNS at 25-dpi EAE (Fig. S6I–K), suggesting that the beneficial function of astrocyte OsmR is not mediated by immune cell numbers. Notably, we found that $Gfap^{cre};Osmr^{fl/fl}$ mice also did not respond to d-zymosan administration as $Osmr^{fl/fl}$ mice did (Fig. 6I, J). Thus, the beneficial effect of Dectin-1 involves OsmR signaling in astrocytes.

Impact of Dectin-1 on EAE is not attributed to hk*Mtb*, used in EAE induction

Next, we sought to determine whether Dectin-1 function in EAE is attributed to the disease induction method which uses hk*Mtb* as an adjuvant. To evaluate whether Dectin-1

recognizes hk*Mtb*, we generated a Dectin-1 signaling reporter cell line (Fig. 7A; S7A). The system showed that zymosan and curdlan both induced robust GFP reporter expression, but hk*Mtb* did not induce GFP expression, even at high concentrations (Fig. 7B, C).

To confirm Dectin-1 was not responding to hk*Mtb* in primary cells, we evaluated *Clec7a*$^{-/-}$ and *Card9*$^{-/-}$ BMDCs. Although *Il1b*, *Il6*, and *Tnf* mRNA expression was reduced in the absence of Card9, the absence of Dectin-1 did not alter expression of the genes upon hk*Mtb* stimulation (Fig. 7D, E). Thus, while Dectin-1 does not detect hk*Mtb*, Card9 mediates response to adjuvant likely through other CLRs upstream of Card9, as previously reported (Fig. S7B) (Miyake et al., 2013; Shenderov et al., 2013; Yonekawa et al., 2014). These results indicate that the beneficial function of Dectin-1 is not attributable to hk*Mtb* adjuvant used in EAE induction but other stimuli, including endogenous Dectin-1 ligands.

Galectin-9 in the CNS limits EAE in a Dectin-1-dependent manner

Next, we sought to evaluate the role of endogenous Dectin-1 ligands in EAE, specifically focusing on reported Dectin-1 ligands, Galectin-9 (Gal-9) (Daley et al., 2017) and Vimentin (Thiagarajan et al., 2013). We found that Gal-9 (*Lgals9*) gene expression was potently upregulated in the SC during EAE to a greater extent than Vimentin (*Vim)* (Fig. 7F). Additionally, reanalyzing data from two independent public data (GSE 108000, 123496) showed that human *LGALS9* mRNA were also elevated in MS brain specimens (Fig. S7C, D), suggesting possible involvement of Gal-9 in MS. These findings led us to test whether Gal-9 stimulation through Dectin-1 could promote *Osm* expression. Indeed, recombinant Gal-9 (rGal9) upregulated expression of *Osm* mRNA in a Dectin-1-dependent manner, at least in part (Fig. S7E). Next, we administered anti-Gal-9 Ab intrathecally at the time of symptom onset (9–15 dpi) and found that blocking Gal-9 led to an increase in EAE severity particularly with impaired remission (Fig. 7G). Thus, we found that Gal-9 in the CNS limits disease during the remission phase of EAE.

Gal-9 limits EAE by inducing T cell apoptosis by ligation of Tim3 on Th1 cells (Zhu et al., 2005). Thus, we tested whether the effect of CNS Gal-9 is mediated also through Dectin-1 in EAE. Intrathecal treatment with Gal-9 Ab exacerbated disease in WT mice but not in *Clec7a*$^{-/-}$ mice (Fig. 7H). Thus, the beneficial effect of Gal-9 in the CNS was dependent on Dectin-1. Together, these findings suggest that Gal-9 may limit EAE not only by acting through Tim3 on T cells, but also by acting as a Dectin-1 ligand on myeloid cells in the CNS.

Next, we considered which cell-types respond to Gal-9 through Dectin-1 in the CNS during EAE. As a previous study indicated astrocytes as a potential source of Gal-9 during inflammation (Steelman and Li, 2014), re-analysis of a published dataset (GSE100330) showed that astrocytes in SC of EAE mice upregulated *Lgals9* mRNA (Fig. S7F). Furthermore, we observed the close proximity between GFAP^{+} astrocytes and Dectin-1^{+} cells, particularly Ly6G^{+} neutrophils, in the SC of EAE mice (Fig. 7I, J). Together, these findings suggest a potential model of bidirectional myeloid cell-astrocyte crosstalk in which (1) Gal-9 produced by astrocytes upregulates Osm via Dectin-1 in myeloid cells and (2) myeloid cell-derived Osm triggers beneficial OsmR signaling in astrocytes.

DISCUSSION

In this study, we found that Dectin-1 limits CNS inflammation in EAE and promotes beneficial myeloid cell-astrocyte crosstalk through Osm-OsmR signaling. Dectin-1 is generally known for its pro-inflammatory response in the setting of fungal infection, particularly by inducing IL-1β via the Card9-NFκB signaling axis and subsequent Th17 cell responses (Gross et al., 2006; LeibundGut-Landmann et al., 2007; Taylor et al., 2007), which are considered to be highly encephalitogenic. Thus, the beneficial role of Dectin-1 in EAE was initially unexpected. We found that Card9-independent Dectin-1 signaling induced expression of the neuroprotective cytokine, *Osm*, and a transcriptional program with protective and anti-inflammatory functions. In humans, eQTLs regulating *CLEC7A* (Dectin-1) gene expression have been identified (Consortium, 2015; Gour et al., 2018) and *CLEC7A* is expressed in active MS lesions (Hendrickx et al., 2017; Voskuhl et al., 2019). Despite the well-known inflammatory role of Dectin-1, some studies have suggested tolerogenic and anti-inflammatory functions of Dectin-1 signaling (Bode et al., 2019; Dillon et al., 2006; Karumuthil-Melethil et al., 2014). Furthermore, Dectin-1 signaling promotes axon regeneration following optic nerve crush injury (Baldwin et al., 2015) and treatment with zymosan (simultaneously stimulates TLR2 and Dectin-1) reduced EAE severity (Li et al., 2013). Thus, harnessing Dectin-1 signaling merits further investigation as a potential therapeutic approach for MS.

We have shown that d-zymosan treatment at 1-dpi delayed EAE onset. To evaluate treatment effects at later timepoints, a d-zymosan *i.v.* injection was performed also at either 9-dpi (onset) or 14-dpi (between onset and peak). However, a majority of mice died within 24 hrs of injection (*unpublished data)*. Reduced amount of d-zymosan from 500 μg to 50 μg per mouse was tried at 9-dpi, but EAE scores were not changed (*unpublished data*). A previous study demonstrates a beneficial response with an injection of zymosan, rather than d-zymosan, at disease onset (100 μg/mouse, *i.p.* route) (Li et al., 2013). Together, certain conditions appeared to be required to achieve the beneficial outcome by Dectin-1 agonist stimulation.

We demonstrated that Dectin-1 did not detect adjuvant, hk*Mtb*. Instead, Card9 rather functioned as a pathogenic integrator of signals from multiple Syk-coupled CLRs aside from Dectin-1 by detecting hk*Mtb*. The function of Dectin-1 in EAE is also unlikely to be attributable to recognition of commensal fungi, because Dectin-1 limited EAE severity even with administration of an oral fluconazole treatment (*data not shown*). While we cannot completely rule out the contribution of microbial ligands, our findings suggest involvement of endogenous Dectin-1 ligands in EAE. Indeed, we found that Gal-9, an endogenous Dectin-1 ligand (Daley et al., 2017), acted in the CNS to limit EAE severity in a Dectin-1-dependent manner. Based on our results and a previous study (Zhu et al., 2005), Gal-9 may act through multiple complementary pathways in EAE through Dectin-1 in myeloid cells and through Tim3 in Th1 cells. Furthermore, other endogenous ligands, Annexin proteins (Bode et al., 2019), Vimentin (Thiagarajan et al., 2013), and various unidentified proteins with N-glycans (Chiba et al., 2014), may also contribute to Dectin-1 signaling. Understanding the role of endogenous Dectin-1 ligands in autoimmunity merits further investigation.

We found that Card9-independent signaling drives expression of *Osm* and other beneficial and anti-inflammatory genes through Syk, PLC, Ca^{2+}, CaN, and NFAT. The existence of multiple Dectin-1 ligands raises the question of whether different ligands could bias Dectin-1 signaling to either a Card9-dependent or Card9-independent pathway. A recent study shows that Dectin-1 signaling triggered by Annexin proteins (endogenous ligands) can induce phosphorylation of Syk at Y348 but not at Y525, while β-glucans (microbial ligand) induce phosphorylation of both sites (Bode et al., 2019). Indeed, Y348 phosphorylation is also triggered by Gal-9 (Daley et al., 2017) and is critical for Syk-induced PLC signaling (Law et al., 1996) which is upstream of NFAT. Here, although Gal-9 can upregulate expression of *Osm* and *Tnf* genes *ex vivo* in bulk neutrophils (*unpublished data*), *Osm* and *Tnf* expression is mutually exclusive in CNS myeloid cells *in vivo* at a single cell level in EAE. Thus, Card9-dependent and independent pathways may not be co-activated in the same cells *in vivo*.

We found that the beneficial function of Dectin-1 was mediated by BM-derived myeloid cells, and CNS-infiltrated neutrophils and monocytes contribute to *Osm* upregulation by Dectin-1 *in vivo* during EAE. Yet, microglia also upregulated Dectin-1 expression in EAE, consistent with the disease-associated microglia (DAM) phenotype (Deczkowska et al., 2018). Although we cannot fully rule out a contribution of microglial Dectin-1 in EAE, neutrophils in particular may be involved, given their abundant infiltration in the CNS during EAE (Caravagna et al., 2018), protective functions in the CNS (Sas et al., 2020), and localization at sites of demyelination and axonal damage in the SC parenchyma during EAE (Carlson et al., 2008; Christy et al., 2013; Soulika et al., 2009; Steinbach et al., 2013; Wu et al., 2010). While the role of neutrophils in MS remains elusive, multiple studies suggest beneficial role of neutrophils, or granulocytic myeloid-derived suppressor cells (G-MDSCs), in both MS and EAE (Casacuberta-Serra et al., 2016; Elliott et al., 2018; Glenn et al., 2019; Hemond et al., 2019; Hertwig et al., 2016; Ioannou et al., 2012; Knier et al., 2018; Liu et al., 2015; Whittaker Hawkins et al., 2017).

We found that Dectin-1 promotes expression of Osm, a cytokine with described protective functions in cuprizone-induced demyelination (Houben et al., 2020; Janssens et al., 2015) and other models of neuropathology (Guo et al., 2015; Slaets et al., 2014). Osm protein is expressed in MS brains (Ruprecht et al., 2001) and is elevated in supernatants of cultured PBMCs from MS patients (Ensoli et al., 2002). In addition, a SNP in the *OSMR* gene was identified as a candidate risk factor for MS (Vandenbroeck et al., 2012). In this study, we found that *Osm* is expressed by myeloid cells in the SC of EAE mice and is upregulated by Dectin-1 signaling. Furthermore, we found that OsmR in astrocytes is beneficial in the remission phase of EAE. While we cannot rule out a role for Dectin-1 in the periphery, our findings demonstrate that Dectin-1 signaling in the CNS promotes myeloid-astrocyte crosstalk through the Osm-OsmR axis to limit EAE. Astrocytes are increasingly recognized as important players in CNS autoimmunity (Voskuhl et al., 2009; Wheeler et al., 2020; Wheeler and Quintana, 2019) and astrocyte gp130, which forms a heterodimer with OsmR, was shown to be protective in EAE (Haroon et al., 2011).

This study contributes to a growing body of evidence that Dectin-1 has important roles beyond the context of fungal infection. We advance this emerging understanding by

identifying a beneficial mechanism of Dectin-1 specifically in the setting of autoimmune neuroinflammation. Together, our findings provoke a reconsideration of Dectin-1 and its functions beyond the context of infection and provide potential targets for therapeutic intervention in neuroinflammatory disorders.

LIMITATIONS OF STUDY

In this study, we identified a beneficial role for Dectin-1 signaling in limiting autoimmune neuroinflammation in the EAE model. However, EAE does not recapitulate all aspects of human CNS autoimmune disease and it remains to be determined whether Dectin-1 is involved in Multiple Sclerosis. In addition, our study has focused primarily on the role of Dectin-1-mediated *Osm* expression in neutrophils and monocytes in the CNS during EAE. However, we do not rule out a role for Dectin-1 in regulating the peripheral immune response during EAE. Future studies using targeted deletion of Dectin-1 (*Clec7a*) in a disease stage and cell type-specific manner will further define the site, timing, and cellular mediators of endogenous Dectin-1 signaling in EAE and may extend the contributions of Dectin-1 signaling in autoimmunity beyond those described in this study.

STAR METHODS

RESOURCE AVAILABILITY

Lead contact: Further information and requests for resources and reagents should be directed to and will be fulfilled by the Lead Contact, Mari L. Shinohara, PhD (mari.shinohara@duke.edu).

Materials Availability: This study did not generate new unique reagents.

Data and Code Availability: Relevant data and materials from this study will be made available upon request. Our RNA sequencing results are available as GSE148850. All custom code will be made available upon request through GitHub.

EXPERIMENTAL MODEL AND SUBJECT DETAILS

Mice—Six- to eight-week old age- and sex-matched mice of the C57BL/6 (B6) background were used for experiments unless otherwise specified. No difference in results between two sexes was found. Dectin-1 deficient ($Clec7a^{-/-}$) mice were originally generated by Dr. Gordon Brown (U. of Aberdeen)(Taylor et al., 2007). $Card9^{-/-}$ mice were provided by Dr. Xin Lin (M.D. Anderson Cancer Center, Houston, TX)(Hsu et al., 2007). $Osmr^{fl/fl}$ mice on a mixed background of B6 and 129×1/SvJ (JAX #011081) were rederived from a cryopreserved line at Jackson Laboratories. We performed speed-congenic approach (DartMouse) to further backcrossed to B6 for 6 additional generations to achieve 99.8 % of the B6 genomic background (Fig. S6H). *Osmr-fl* mice were then crossed to $Gfap^{cre}$ (JAX #024098), and littermate controls were used for $Osmr^{fl/fl}$ experiments. Fixed tissues from *Aldh1l1-eGFP* mice (MMRRC #011015-UCD) were provided by the laboratory of Dr. Cagla Eroglu (Duke U.). All mice were housed under specific pathogen-free conditions and all animal experiments were performed as approved by Institutional Animal Care and Use Committee at Duke University.

Dectin-1 reporter cell line—A retroviral plasmid pMXs-IP-mCD3ζ-mDectin1 vector (Pyz et al., 2008), a gift from Gordon Brown (U. of Aberdeen, UK) and Pcl-Eco (packaging vector) were transfected to BOSC cells using lipofectamine LTX to generate retrovirus for gene transfection. The mCD3ζ-mDectin1 fusion protein was expressed in the TCR-negative 58α$^-$β$^-$ mouse T hybridoma, expressing GFP upon mCD3ζ activation (Ise et al., 2010) (gift from Ken Murphy, Washington U.). Activated Dectin-1 was reported by GFP expression by the hybridoma and detected by flow cytometry. Cell lines used in this study did not undergo authentication in our laboratory.

METHOD DETAILS

Reagents, Abs, and recombinant proteins—Curdlan (β−1,3 glucan hydrate, from *Alcaligenes faecalis*, Sigma-Aldrich) was used as a Dectin-1 specific agonist for *ex vivo* experiments, unless otherwise indicated. Hot-alkali treated depleted zymosan (dz) (InvivoGen) was used as a Dectin-1-specific ligand for *in vivo* experiments. Heat-killed *Mycobacterium tuberculosis* (hk*Mtb*) H37a Ra was purchased from BD Difco™. Small molecule signaling inhibitors were purchased from Cayman Chemical, with the exception of GW5074 (Sigma Aldrich), and concentrations for their use were determined using supplier recommendations and based on previous publications. Recombinant mouse (rm) M-CSF and GM-CSF proteins were obtained from BioLegend. Recombinant mouse Gal-9 was obtained from R&D. $MOG_{35–55}$ peptide (MEVGWYRSPFSRVVHLYRNGK) was synthesized by United Biosystems. Enzyme-linked immunosorbent assay (ELISA) kits for detection of mouse Osm were purchased from R&D, and ELISA kit for detection of mouse IL-10 was purchased from BioLegend. Detailed list of Abs and reagents can be found in the Key Resources Table.

EAE induction and evaluation—Unless otherwise noted, EAE was induced as follows: $MOG_{35–55}$ peptide (100 μg in 100 μl PBS) emulsified in CFA (100 μl including 2 mg/ml hk*Mtb*) was subcutaneously (*s.c.*) injected into lower flanks of mice. Intraperitoneal injection of pertussis toxin (List Biologicals; 200 ng in 200 μl PBS) was performed on day 0 and 2. EAE induction was performed with reduced adjuvant in Fig. 1B, Fig. 3E, F, and Fig. 7H by using 0.5 mg/ml instead of 2 mg/ml hk*Mtb* CFA (*i.e.*, 50 μg/mouse instead of 200 μg/mouse). Mice were monitored daily for clinical signs of EAE and scores were assigned based on the following criteria: 0.5, partial tail limpness; 1, tail limpness; 1.5, impaired righting reflex; 2, partial hindlimb paralysis; 2.5, partial hindlimb paralysis with dragging of at least one hind paw; 3, bilateral hindlimb paralysis; 3.5, severe bilateral hindlimb paralysis with hunched posture; 4, hind- and forelimb paralysis; 5, death.

Cell isolation for flow cytometry analysis—Mice were euthanized with CO_2 in addition to a secondary method, as recommended by American Veterinary Medical Association. BM was isolated from the femur and tibia by flushing marrow with a needle and syringe filled with sterile PBS and pipetting to obtain a single cell suspension. Spleens and ILNs were dissected and homogenized using sterile glass slides. SC cells were isolated by flushing the SC from the vertebral column with a needle and syringe filled with sterile PBS, minced in PBS including 5% FBS and 1mM HEPES, then digested with Collagenase D (Roche) at 37 C for 30 minutes. Following digestion, single cell suspensions were

prepared by passing through an 18G needle and filtered through a 70 μm cell strainer. Cells were then resuspended in 38 % isotonic Percoll and centrifuged at 2,000 g for 30 min with no brake. Following centrifugation, the lipid and debris layer was aspirated from the top of the tube and the cell pellet was resuspended. All tissues were treated with RBC lysis solution prior to staining for flow cytometry.

Ab staining for flow cytometry—Analyses for live cells was performed using a LIVE/DEAD™ fixable dead cell stain kit (Invitrogen) prior to staining with fluorochrome-conjugated Abs, listed in the Key Resources Table, by flow cytometry using either Fortessa X20 or FACSCanto (BD systems). Results were analyzed using the FlowJo software. Specific cell types were gated as neutrophils ($CD11b^+Ly6G^+$), monocytes ($CD11b^+Ly6G^-Ly6C^{hi}$), cDCs ($CD11b^+CD11c^+$, with $MHC\text{-}II^{hi}$ for some experiments), $F4/80^{hi}$ macrophages ($CD11b^+F4/80^{hi}$), B cells ($CD19^+$), $CD4^+$ T cells ($CD3^+CD4^+$), $CD8^+$ T cells ($CD3^+CD8^+$), microglia ($CD45^{lo}CD11b^{lo}$ and $Tmem119^+$, as indicated in the text).

PrimeFlow mRNA detection—Cells from the SC of EAE mice were isolated using the methods described above with LIVE/DEAD™ staining and fluorochrome-conjugated Abs for cell-surface markers. *In situ* hybridization for *Osm* mRNA was performed using the PrimeFlow RNA Assay Kit (Invitrogen) according to manufacturer's instructions. Cells were analyzed by flow cytometry using Fortessa X20 (BD systems) and results were analyzed using the FlowJo software.

Intracellular cytokine staining for flow cytometry—Intracellular cytokine staining was performed on spleen and LN single cell suspensions following 6 hr stimulation with PMA (10ng/ml) (Sigma Aldrich) and ionomycin (1μg/ml) (Sigma Aldrich), with GolgiPlug (BD) in the final 4 hrs of stimulation. Staining was performed using a LIVE/DEAD™ staining followed by fluorochrome-conjugated Abs for cell surface proteins before fixation and permeabilization (BD Cytofix/Cytoperm Kit). Ab staining for intracellular cytokines was then performed in permeabilization buffer. Intracellular staining for Foxp3 was performed on single cell suspensions from spleen and LNs specifically using a FOXP3 Fix/Perm Kit (BioLegend).

T cell recall response assay—Lymph node $CD4^+$ T cells from EAE mice were enriched using a $CD4^+$ T cell negative selection kit (StemCell Technologies). Splenic $CD11c^+$ cells from WT naïve mice were enriched using MACS-column purification (Miltenyi Biotec) with biotinylated mouse CD11c Abs (BioLegend) and streptavidin magnetic beads (Miltenyi Biotec). $CD11c^+$ cells and $CD4^+$ T cells were co-cultured at a 1:1 ratio in complete RPMI with 10 μg/ml $MOG_{35–55}$ peptide. Cells were also labeled with CellTrace Violet (ThermoFisher) proliferation dye prior to co-culture. After 3 days, cells were collected to detect dilution of the proliferation dye by flow-cytometry as shown in Fig. S3K.

IL-10 expression by $CD25^+CD4^+$ T cells—Splenic $CD4^+$ T cells from EAE mice were enriched using a $CD4^+$ T cell negative selection kit (StemCell Technologies) according to manufacturer's instructions. $CD25^+$ cells were subsequently isolated from the $CD4^+$ T cell pool using MACS-column purification (Miltenyi Biotec) with biotinylated mouse CD25 Abs (BioLegend) and streptavidin magnetic beads (Miltenyi Biotec). Isolated $CD25^+CD4^+$ T

cells were cultured with “Mouse T-activator CD3/CD28” Dynabeads (Gibco) in complete RPMI. Supernatants were collected after 3 days and tested for IL-10 protein quantitation by ELISA (BioLegend).

Neutrophil, monocyte, and BM-derived cell culture—BM neutrophils were isolated using MACS-column purification (Miltenyi Biotec) with biotinylated mouse Ly6G Abs (BioLegend) and streptavidin magnetic beads (Miltenyi Biotec) for *ex vivo* study. BM monocytes, were isolated by flow cytometry-sorting as $CD11b^{+}Ly6G^{-}Ly6C^{+}$ cells (Astrios sorter, Beckman Coulter). When neutrophils were compared to monocytes, flow cytometry-sorting was used to isolate neutrophils as $CD11b^{+}Ly6G^{+}$. BMDMs and BMDCs were generated by culturing BM cells with rmM-CSF (20 ng/ml, BioLegend) and rmGM-CSF (20 ng/ml, BioLegend), respectively. Complete RPMI medium was used for all cell culture studies.

Isolation of spinal cord tissue for histology—Transcardial perfusion was used to maximize integrity of brain and SC tissue to improve sample quality. Specifically, mice were administered sodium pentobarbital (100 mg/kg) by intraperitoneal injection and monitored until complete anesthesia was achieved (non-responsive to pedal reflex). The thoracic cavity was dissected, and the inferior vena cava severed prior to insertion of a needle in the left ventricle and slow manual administration of PBS followed by 4% paraformaldehyde (PFA). Following transcardial perfusion and fixation, spinal cord tissue was manually dissected and fixed in 4% PFA overnight before cryoprotection in 30% sucrose for 1–2 days. Tissues were embedded in Tissue-Tek OCT compound (Sakura), frozen, and stored at −80 °C.

LFB-PAS staining and imaging—Luxol fast blue (LFB)-Periodic Acid Schiff (PAS) staining was performed on transverse fixed-frozen sections (10 μm) of lumbar spinal cord using LFB Solvent blue 38, Gill’s Hematoxylin No. 3, and Schiff’s reagent (all obtained from Sigma-Aldrich). LFB-PAS stained sections were imaged on the Zeiss Axio Imager widefield microscope.

Immunofluorescent staining and imaging—Staining was performed with either floating sections in tissue culture wells or thaw-mounted sections on slides. Transverse fixed-frozen sections (25 μm) of lumbar spinal cord were washed with TBS-T, permeabilized with TBS 0.25% Triton 1× for 15min, washed with TBS-T, then incubated in blocking buffer (TBS-T 3% BSA) for at least 1 hr. Primary Ab staining was performed overnight at 4 °C, followed by washing in TBS-T. Secondary Ab staining with fluorochrome-conjugated Abs was performed for 2 hrs at 4 °C (Abs listed in Key Resources Table). Stained sections were washed and mounted using ProLong Gold Antifade Mountant with DAPI (ThermoFisher). Slides were imaged using the Zeiss 710 inverted confocal microscope and analyzed using ImageJ. IF images are typically representative of at least two high-power field (hpf) per sample, and data was obtained from several individual animals per experiment (sample size (n) denoting number of mice).

mRNA detection in tissue sections by RNAscope—To prepare samples for RNAscope, lumbar SC segments were dissected following transcardial perfusion (described above) and post-fixed overnight in 4% PFA. Samples were then transferred to 30% sucrose

in PBS and kept overnight. Spinal cords were cryosectioned to 20 μm and thaw-mounted onto Superfrost Plus slides (Fisher Scientific). Slides were allowed to dry for 20 minutes at room temperature, and then stored at −20 C overnight. The RNAscope Multiplex Fluorescent Reagent Kit v2 (Advanced Cell Diagnostics, ACD) was used for *in situ* hybridization as previously described (Chamessian et al., 2018). Tissue pretreatment was performed for 30 min with Protease IV in the RNAscope kit at RT followed by probe hybridization and detection according to manufacturer's instructions. We used probes designed by Advanced Cell Diagnostics to *Osm* (NM_001013365.2), specifically Mm-Osm (#427071). IF staining with Ab to CD11b was performed after the RNAscope procedure using methods described above. Slides were imaged using the Zeiss 710 inverted confocal microscope. For comparison of naïve and EAE conditions, *Osm* mRNA puncta were quantified by performing object detection using ImageJ, calculating the integrated density for each punctum, and summing over all puncta in a given 350 μm^2 hpf. Positive signal, *i.e.*, puncta, was defined as >5-fold higher than background. Five hpf per mouse were analyzed, one in each indicated region of lumbar SC. For evaluation of *Osm* expression in $CD11b^+$ cells, z-stack images with 1.16 μm spacing were collected through the full thickness of each section. For each 350 μm^2 ventrolateral white matter hpf per mouse, *Osm* puncta were quantified manually in a blinded manner. Specifically, *Osm* puncta per $CD11b^+$ cell were quantified by examining multiple z-stacks in 3D space to identify cell-associated puncta.

RT-qPCR analysis—To evaluate gene expression in *ex vivo* stimulation experiments, total RNA was extracted from cells with TRIzol on purified cells, while RNeasy Micro Kit (Qiagen) was used for flow cytometry-sorted cells. cDNA synthesis was performed using qScript cDNA Mix (Quantabio). Real-time, quantitative polymerase chain reaction (RT-qPCR) was performed with SYBR FAST qPCR Master Mix (Kapa Biosystems) with primers shown in Table S1. Relative amounts of qPCR product were determined using the $-\Delta\Delta Ct$ method (Livak and Schmittgen, 2001) comparing relative expression of housekeeping (*Actb)* and target genes. Error bars denote mean ± SEM of biological replicates in Fig. 4A, B; Fig. 5A; Fig. 7D, F; Fig. S4G–I; and Fig. S7E. In Figures 4D, Fig. 5L, N, O; Fig. S4F; and Fig. S5A–D, F error bars (sometimes too short to be identified) were calculated using RQ-Min = $2^{-(\Delta\Delta Ct + \mathrm{T} * \mathrm{SD}(\Delta Ct))}$ and RQ-Max = $2^{-(\Delta\Delta Ct - \mathrm{T} * \mathrm{SD}(\Delta Ct))}$ from triplicate wells as suggested by Applied Biosystems (manufacturer of qPCR machines). Results shown are representative of multiple independent experiments with similar results.

RNA-sequencing—BM neutrophils were obtained by MACS-column purification as described above. Each sample was obtained from an individual WT or $Card9^{-/-}$ mouse (n=3). Cells were stimulated for 3 hrs with curdlan (100 μg/ml). Total RNA was extracted from cells using the RNeasy Micro Kit (Qiagen). mRNA libraries were prepared using the KAPA stranded mRNA-seq kit by Duke Sequencing and Genomic Technologies Shared Resource facility. RNA libraries were sequenced on an Illumina HiSeq4000 using 50-bp single reads.

Experimental design—Sample sizes for animal experiments were selected with goal of minimizing animal numbers while maintaining sufficient power to detect biologically significant effects in statistical analysis of data from multiple replicate experiments.

Although statistical tests were not used to determine sample size, we always repeated experiments and ran statistics to draw conclusions. No data points were excluded from figures in this manuscript. As indicated in the text or figure legend, all figures are from either one experiment representative of multiple replicate experiments or include data from multiple replicate experiments combined into a single figure. Definition of sample size (*n*) is indicated in figure legends. Mouse experiments were performed with age- and sex-matching of individuals in each experimental condition to reduce the effect of these biological covariates, and randomization of individual animals to treatment conditions was performed when feasible. Investigator blinding was performed for quantitative image analysis of *in situ* hybridization data and for animal experiments which used littermate controls.

QUANTIFICATION AND STATISTICAL ANALYSIS

Statistical analysis—EAE clinical scores were analyzed by calculating the area under the curve (AUC) summing clinical scores over the indicated period. Statistical analysis of EAE clinical score AUC was performed using a non-parametric Mann-Whitney U-test and, where indicated, AUC was normalized to the mean of the control group. Box plots of EAE clinical score AUC data include the following elements: center line, median; box limits, upper and lower quartiles; whiskers, minimum and maximum values. For remaining analyses, student's t-test (paired or unpaired, as appropriate, two-sided in all cases) or analysis of variance (ANOVA) was applied (one- or two-factors, repeated measures as appropriate) as indicated in figure legends. If a two-factor ANOVA yielded an interaction term with $p<0.1$, then post-hoc Sidak testing with correction for multiple comparison was applied. If a two-factor ANOVA did not result in a significant interaction term ($p>0.1$), then any significant main effects are indicated in the figure and legend. Log-transformation was performed prior to 2-factor ANOVA as appropriate when data include values that varied greatly in magnitude between multiple cell types (Fig. 2F, G; Fig. 4A,B; Fig. S1E, F, H, I; Fig. S2B, C; Fig. S3G; Fig. S6I–K). All results are expressed as means ± SEM unless otherwise noted, and criterion of significance was set as $p<0.05$ (*), $p<0.01$ (**), or $p<0.001$ (***). Apart from analysis of RNA-seq data (described below), Microsoft Excel and GraphPad Prism software were used for all statistical analyses.

Flow cytometry analysis—Flow cytometry analysis was performed using a BD FACSCanto II or BD Fortessa X-20 analyzer. Flow cytometry sorting was performed using B-C Astrios sorters. FlowJo software was used to analyze all flow cytometry data in this study. For all flow cytometry sorting experiments, at least one representative post-sort sample was re-analyzed for cell purity based on original markers before proceeding with further sample processing. All flow cytometry analysis in this study used: (1) an initial FSC-A/SSC-A gate to eliminate low FSC-A/SSC-A debris, (2) a FSC-H/FSC-A gate to identify single cells, and (3) Fixable Live/Dead stains to identify live cells for further analysis All gating strategies are described in the text where indicated.

RNA-seq analysis—Initial processing and analysis of sequencing results was performed by Duke Genomic Analysis and Bioinformatics core facility as described here: RNA-seq data was processed using the TrimGalore toolkit which employs Cutadapt (Martin, 2011) to trim low-quality bases and Illumina sequencing adapters from the 3' end of the reads. Only

reads that were 20nt or longer after trimming were kept for further analysis. Reads were mapped to the GRCm38v73 version of the mouse genome and transcriptome (Kersey et al., 2012) using the STAR RNA-seq alignment tool (Dobin et al., 2013). Reads were kept for subsequent analysis if they mapped to a single genomic location. Gene counts were compiled using the HTSeq tool. Only genes that had at least 10 reads in any given library were used in subsequent analysis. Normalization and differential expression was carried out using the DESeq2 (Love et al., 2014) Bioconductor (Huber et al., 2015) package with the R statistical programming environment (Team, 2013) (Table S2). The false discovery rate was calculated to control for multiple hypothesis testing.

Card9-dependent and -independent candidate genes—We first selected genes with significant differential expression following curdlan stimulation in WT neutrophils (log_2 fold-change >|1.5| and adjusted p-value<0.05). Among statistically significant differentially expressed genes, we then selected Card9-dependent candidate genes (adjusted p-value < 0.05 for interaction of genotype and stimulation). Among the remaining genes, (adjusted p-value > 0.05 for interaction of genotype and stimulation), we further selected those genes with a stimulation-induced fold-change within 30 % of WT values (1 ± 0.3) and defined these as Card9-independent candidate genes (Table S3).

Reactome pathway enrichment analysis—Using these Card9-dependent and -independent candidate gene lists, we performed pathway enrichment analysis on those genes that are upregulated with curdlan stimulation using the *ReactomePA* package and gene set overlap analysis (Yu and He, 2016) (Table S3) and plotted the resulting enriched pathways (adjusted p-value < 0.05) using a *cnetplot* network diagram (genes are small grey points, pathways are colored, lines indicate correspondence of genes with pathways).

Transcription factor enrichment analysis—To identify potential transcription factors that may regulate Card9-dependent and -independent candidate genes, we developed an analysis approach which leverages existing datasets and tools. Our goal was to identify potential TF candidates based on predicted binding sites near genes in either the Card9-dependent or -independent candidate gene lists. We limited our analysis of predicted binding sites to OCRs in our cell type of interest (BM neutrophils) to better target relevant sites for possible TF binding. We obtained analyzed ATAC-seq result files from ImmGen for BM neutrophils which contained information on each OCR, an OCR score for the particular cell type, predicted TF binding sites within each OCR, and genes within 100 kb of each OCR (Heng et al., 2008; Yoshida et al., 2019) (downloaded from Immgen site on May 22nd, 2019). From this genome-wide dataset, we selected only OCRs with a score of >10 in BM neutrophils to specifically include regions of open chromatin in our analysis. From these OCRs, we generated a paired list of TFs (with predicted binding sites within a given OCR) and genes (within 100 kb of a given OCR). This paired list was then used as a custom reference for gene set overlap analysis, in which the category is a given TF. Then we used *GOseq* (Young et al., 2010) to perform gene set overlap analysis between either Card9-dependent or -independent genes and our custom reference. Benjamini Hochberg adjusted p-values were obtained for each TF category for either Card9-dependent or -independent genes (Table S3). We then plotted the - log(adjusted p-value) for each TF on a violin plot and

labeled TFs in the NFκB or NFAT families (Fig. 5H, I). In addition, we plotted a Venn diagram of genes with at least 3 predicted binding sites of either NFκB or NFAT family TFs (within 100 kb of gene) (Fig. 5J)

Supplementary Material

Refer to Web version on PubMed Central for supplementary material.

ACKNOWLEDGEMENTS

Funding: This study was funded by the National Multiple Sclerosis Society (Pilot Grant PP-1509-06274; Research Grant RG 4536B2/1), the NIH (R01-AI088100) to M.L.S. and the NIH (F30-AI140497, T32-GM007171) to M.E.D.

We appreciate the assistance of the Duke Center for Genomic and Computational Biology core facility and the Duke Cancer Institute Flow Cytometry Core, particularly Lynn Martinek. Christabel Tan in the laboratory of Cagla Eroglu (Duke U.) provided samples from *Aldh1l1-eGFP* mice. Gordon Brown (U. of Aberdeen, UK) provided the pMXs-IP-mCD3ζ - mDectin1 construct under MTA. Ken Murphy (Washington U.) provided the 58α^{-}β^{-} mouse T hybridoma cell line with stable expression of a NFAT-GFP-hCD4 RV reporter construct. Megumi Matsuda, Qianru He, and Zilong Wang, in the laboratory of Ru Rong Ji (Duke U.) provided assistance with RNAscope *in situ* hybridization. Tomoko Kadota and Tamira-Marie Bickems in Shinohara Lab provided assistance with mouse genotyping.

REFERENCES

Baldwin KT, Carbajal KS, Segal BM, and Giger RJ (2015). Neuroinflammation triggered by beta-glucan/dectin-1 signaling enables CNS axon regeneration. Proc Natl Acad Sci U S A 112, 2581–2586. [PubMed: 25675510]

Bode K, Bujupi F, Link C, Hein T, Zimmermann S, Peiris D, Jaquet V, Lepenies B, Weyd H, and Krammer PH (2019). Dectin-1 Binding to Annexins on Apoptotic Cells Induces Peripheral Immune Tolerance via NADPH Oxidase-2. Cell Rep 29, 4435–4446 e4439. [PubMed: 31875551]

Brown BR, Lee EJ, Snow PE, Vance EE, Iwakura Y, Ohno N, Miura N, Lin X, Brown GD, Wells CA, et al. (2017). Fungal-derived cues promote ocular autoimmunity through a Dectin-2/Card9-mediated mechanism. Clin Exp Immunol 190, 293–303. [PubMed: 28763100]

Caravagna C, Jaouen A, Desplat-Jego S, Fenrich KK, Bergot E, Luche H, Grenot P, Rougon G, Malissen M, and Debarbieux F (2018). Diversity of innate immune cell subsets across spatial and temporal scales in an EAE mouse model. Sci Rep 8, 5146. [PubMed: 29572472]

Carlson T, Kroenke M, Rao P, Lane TE, and Segal B (2008). The Th17-ELR+ CXC chemokine pathway is essential for the development of central nervous system autoimmune disease. The Journal of experimental medicine 205, 811–823. [PubMed: 18347102]

Casacuberta-Serra S, Costa C, Eixarch H, Mansilla MJ, Lopez-Estevez S, Martorell L, Pares M, Montalban X, Espejo C, and Barquinero J (2016). Myeloid-derived suppressor cells expressing a self-antigen ameliorate experimental autoimmune encephalomyelitis. Exp Neurol 286, 50–60. [PubMed: 27693617]

Chamessian A, Young M, Qadri Y, Berta T, Ji RR, and Van de Ven T (2018). Transcriptional Profiling of Somatostatin Interneurons in the Spinal Dorsal Horn. Sci Rep 8, 6809. [PubMed: 29717160]

Chiba S, Ikushima H, Ueki H, Yanai H, Kimura Y, Hangai S, Nishio J, Negishi H, Tamura T, Saijo S, et al. (2014). Recognition of tumor cells by Dectin-1 orchestrates innate immune cells for anti-tumor responses. Elife 3, e04177. [PubMed: 25149452]

Christy AL, Walker ME, Hessner MJ, and Brown MA (2013). Mast cell activation and neutrophil recruitment promotes early and robust inflammation in the meninges in EAE. J Autoimmun 42, 50–61. [PubMed: 23267561]

Consortium GT (2015). Human genomics. The Genotype-Tissue Expression (GTEx) pilot analysis: multitissue gene regulation in humans. Science 348, 648–660. [PubMed: 25954001]

Daley D, Mani VR, Mohan N, Akkad N, Ochi A, Heindel DW, Lee KB, Zambirinis CP, Pandian GSB, Savadkar S, et al. (2017). Dectin 1 activation on macrophages by galectin 9 promotes pancreatic carcinoma and peritumoral immune tolerance. Nat Med 23, 556–567. [PubMed: 28394331]

Deczkowska A, Keren-Shaul H, Weiner A, Colonna M, Schwartz M, and Amit I (2018). Disease-Associated Microglia: A Universal Immune Sensor of Neurodegeneration. Cell 173, 1073–1081. [PubMed: 29775591]

Deerhake ME, Biswas DD, Barclay WE, and Shinohara ML (2019). Pattern Recognition Receptors in Multiple Sclerosis and Its Animal Models. Front Immunol 10, 2644. [PubMed: 31781124]

Dendrou CA, Fugger L, and Friese MA (2015). Immunopathology of multiple sclerosis. Nat Rev Immunol 15, 545–558. [PubMed: 26250739]

Dillon S, Agrawal S, Banerjee K, Letterio J, Denning TL, Oswald-Richter K, Kasprowicz DJ, Kellar K, Pare J, van Dyke T, et al. (2006). Yeast zymosan, a stimulus for TLR2 and dectin-1, induces regulatory antigen-presenting cells and immunological tolerance. J Clin Invest 116, 916–928. [PubMed: 16543948]

Dobin A, Davis CA, Schlesinger F, Drenkow J, Zaleski C, Jha S, Batut P, Chaisson M, and Gingeras TR (2013). STAR: ultrafast universal RNA-seq aligner. Bioinformatics 29, 15–21. [PubMed: 23104886]

Elliott DM, Singh N, Nagarkatti M, and Nagarkatti PS (2018). Cannabidiol Attenuates Experimental Autoimmune Encephalomyelitis Model of Multiple Sclerosis Through Induction of Myeloid-Derived Suppressor Cells. Front Immunol 9, 1782. [PubMed: 30123217]

Ensoli F, Fiorelli V, Lugaresi A, Farina D, De Cristofaro M, Collacchi B, Muratori DS, Scala E, Di Gioacchino M, Paganelli R, and Aiuti F (2002). Lymphomononuclear cells from multiple sclerosis patients spontaneously produce high levels of oncostatin M, tumor necrosis factors alpha and beta, and interferon gamma. Mult Scler 8, 284–288. [PubMed: 12166497]

Gadani SP, Walsh JT, Lukens JR, and Kipnis J (2015). Dealing with Danger in the CNS: The Response of the Immune System to Injury. Neuron 87, 47–62. [PubMed: 26139369]

Gensel JC, Wang Y, Guan Z, Beckwith KA, Braun KJ, Wei P, McTigue DM, and Popovich PG (2015). Toll-Like Receptors and Dectin-1, a C-Type Lectin Receptor, Trigger Divergent Functions in CNS Macrophages. J Neurosci 35, 9966–9976. [PubMed: 26156997]

Glenn JD, Liu C, and Whartenby KA (2019). Frontline Science: Induction of experimental autoimmune encephalomyelitis mobilizes Th17-promoting myeloid derived suppressor cells to the lung. J Leukoc Biol 105, 829–841. [PubMed: 30762897]

Goodridge HS, Simmons RM, and Underhill DM (2007). Dectin-1 stimulation by Candida albicans yeast or zymosan triggers NFAT activation in macrophages and dendritic cells. J Immunol 178, 3107–3115. [PubMed: 17312158]

Gour N, Lajoie S, Smole U, White M, Hu D, Goddard P, Huntsman S, Eng C, Mak A, Oh S, et al. (2018). Dysregulated invertebrate tropomyosin-dectin-1 interaction confers susceptibility to allergic diseases. Sci Immunol 3.

Griffiths MR, Botto M, Morgan BP, Neal JW, and Gasque P (2018). CD93 regulates central nervous system inflammation in two mouse models of autoimmune encephalomyelitis. Immunology 155, 346–355. [PubMed: 29923617]

Gross O, Gewies A, Finger K, Schafer M, Sparwasser T, Peschel C, Forster I, and Ruland J (2006). Card9 controls a non-TLR signalling pathway for innate anti-fungal immunity. Nature 442, 651–656. [PubMed: 16862125]

Guo S, Li ZZ, Gong J, Xiang M, Zhang P, Zhao GN, Li M, Zheng A, Zhu X, Lei H, et al. (2015). Oncostatin M Confers Neuroprotection against Ischemic Stroke. J Neurosci 35, 12047–12062. [PubMed: 26311783]

Haroon F, Drogemuller K, Handel U, Brunn A, Reinhold D, Nishanth G, Mueller W, Trautwein C, Ernst M, Deckert M, and Schluter D (2011). Gp130-dependent astrocytic survival is critical for the control of autoimmune central nervous system inflammation. J Immunol 186, 6521–6531. [PubMed: 21515788]

Hemond CC, Glanz BI, Bakshi R, Chitnis T, and Healy BC (2019). The neutrophil-to-lymphocyte and monocyte-to-lymphocyte ratios are independently associated with neurological disability and brain atrophy in multiple sclerosis. BMC Neurol 19, 23. [PubMed: 30755165]

Hendrickx DAE, van Scheppingen J, van der Poel M, Bossers K, Schuurman KG, van Eden CG, Hol EM, Hamann J, and Huitinga I (2017). Gene Expression Profiling of Multiple Sclerosis Pathology Identifies Early Patterns of Demyelination Surrounding Chronic Active Lesions. Front Immunol 8, 1810. [PubMed: 29312322]

Heng TS, Painter MW, and Immunological Genome Project C (2008). The Immunological Genome Project: networks of gene expression in immune cells. Nat Immunol 9, 1091–1094. [PubMed: 18800157]

Hertwig L, Pache F, Romero-Suarez S, Sturner KH, Borisow N, Behrens J, Bellmann-Strobl J, Seeger B, Asselborn N, Ruprecht K, et al. (2016). Distinct functionality of neutrophils in multiple sclerosis and neuromyelitis optica. Mult Scler 22, 160–173. [PubMed: 26540731]

Houben E, Hellings N, and Broux B (2019). Oncostatin M, an Underestimated Player in the Central Nervous System. Front Immunol 10, 1165. [PubMed: 31191538]

Houben E, Janssens K, Hermans D, Vandooren J, Van den Haute C, Schepers M, Vanmierlo T, Lambrichts I, van Horssen J, Baekelandt V, et al. (2020). Oncostatin M-induced astrocytic tissue inhibitor of metalloproteinases-1 drives remyelination. Proc Natl Acad Sci U S A 117, 5028–5038. [PubMed: 32071226]

Hsu YM, Zhang Y, You Y, Wang D, Li H, Duramad O, Qin XF, Dong C, and Lin X (2007). The adaptor protein CARD9 is required for innate immune responses to intracellular pathogens. Nat Immunol 8, 198–205. [PubMed: 17187069]

Huber W, Carey VJ, Gentleman R, Anders S, Carlson M, Carvalho BS, Bravo HC, Davis S, Gatto L, Girke T, et al. (2015). Orchestrating high-throughput genomic analysis with Bioconductor. Nat Methods 12, 115–121. [PubMed: 25633503]

Ikeda Y, Adachi Y, Ishii T, Miura N, Tamura H, and Ohno N (2008). Dissociation of Toll-like receptor 2-mediated innate immune response to Zymosan by organic solvent-treatment without loss of Dectin-1 reactivity. Biol Pharm Bull 31, 13–18. [PubMed: 18175935]

Ioannou M, Alissafi T, Lazaridis I, Deraos G, Matsoukas J, Gravanis A, Mastorodemos V, Plaitakis A, Sharpe A, Boumpas D, and Verginis P (2012). Crucial role of granulocytic myeloid-derived suppressor cells in the regulation of central nervous system autoimmune disease. J Immunol 188, 1136–1146. [PubMed: 22210912]

Ise W, Kohyama M, Nutsch KM, Lee HM, Suri A, Unanue ER, Murphy TL, and Murphy KM (2010). CTLA-4 suppresses the pathogenicity of self antigen-specific T cells by cell-intrinsic and cell-extrinsic mechanisms. Nat Immunol 11, 129–135. [PubMed: 20037585]

Janssens K, Maheshwari A, Van den Haute C, Baekelandt V, Stinissen P, Hendriks JJ, Slaets H, and Hellings N (2015). Oncostatin M protects against demyelination by inducing a protective microglial phenotype. Glia 63, 1729–1737. [PubMed: 25921393]

Karumuthil-Melethil S, Gudi R, Johnson BM, Perez N, and Vasu C (2014). Fungal beta-glucan, a Dectin-1 ligand, promotes protection from type 1 diabetes by inducing regulatory innate immune response. J Immunol 193, 3308–3321. [PubMed: 25143443]

Kersey PJ, Staines DM, Lawson D, Kulesha E, Derwent P, Humphrey JC, Hughes DS, Keenan S, Kerhornou A, Koscielny G, et al. (2012). Ensembl Genomes: an integrative resource for genome-scale data from non-vertebrate species. Nucleic Acids Res 40, D91–97. [PubMed: 22067447]

Knier B, Hiltensperger M, Sie C, Aly L, Lepennetier G, Engleitner T, Garg G, Muschaweckh A, Mitsdorffer M, Koedel U, et al. (2018). Myeloid-derived suppressor cells control B cell accumulation in the central nervous system during autoimmunity. Nat Immunol 19, 1341–1351. [PubMed: 30374128]

Larochelle A, Bellavance MA, Michaud JP, and Rivest S (2016). Bone marrow-derived macrophages and the CNS: An update on the use of experimental chimeric mouse models and bone marrow transplantation in neurological disorders. Biochim Biophys Acta 1862, 310–322. [PubMed: 26432480]

Law CL, Chandran KA, Sidorenko SP, and Clark EA (1996). Phospholipase C-gamma1 interacts with conserved phosphotyrosyl residues in the linker region of Syk and is a substrate for Syk. Mol Cell Biol 16, 1305–1315. [PubMed: 8657103]

Lee EJ, Brown BR, Vance EE, Snow PE, Silver PB, Heinrichs D, Lin X, Iwakura Y, Wells CA, Caspi RR, and Rosenzweig HL (2016). Mincle Activation and the Syk/Card9 Signaling Axis Are Central

to the Development of Autoimmune Disease of the Eye. J Immunol 196, 3148–3158. [PubMed: 26921309]

LeibundGut-Landmann S, Gross O, Robinson MJ, Osorio F, Slack EC, Tsoni SV, Schweighoffer E, Tybulewicz V, Brown GD, Ruland J, and Reis e Sousa C (2007). Syk- and CARD9-dependent coupling of innate immunity to the induction of T helper cells that produce interleukin 17. Nat Immunol 8, 630–638. [PubMed: 17450144]

Li H, Gonnella P, Safavi F, Vessal G, Nourbakhsh B, Zhou F, Zhang GX, and Rostami A (2013). Low dose zymosan ameliorates both chronic and relapsing experimental autoimmune encephalomyelitis. J Neuroimmunol 254, 28–38. [PubMed: 23010280]

Liu Y, Holdbrooks AT, Meares GP, Buckley JA, Benveniste EN, and Qin H (2015). Preferential Recruitment of Neutrophils into the Cerebellum and Brainstem Contributes to the Atypical Experimental Autoimmune Encephalomyelitis Phenotype. J Immunol 195, 841–852. [PubMed: 26085687]

Livak KJ, and Schmittgen TD (2001). Analysis of relative gene expression data using real-time quantitative PCR and the 2(-Delta Delta C(T)) Method. Methods 25, 402–408. [PubMed: 11846609]

Love MI, Huber W, and Anders S (2014). Moderated estimation of fold change and dispersion for RNA-seq data with DESeq2. Genome Biol 15, 550. [PubMed: 25516281]

Martin M (2011). Cutadapt removes adapter squences from high-throughput sequencing reads. Bioinf. in action 17, 10–12.

Miyake Y, Toyonaga K, Mori D, Kakuta S, Hoshino Y, Oyamada A, Yamada H, Ono K, Suyama M, Iwakura Y, et al. (2013). C-type lectin MCL is an FcRgamma-coupled receptor that mediates the adjuvanticity of mycobacterial cord factor. Immunity 38, 1050–1062. [PubMed: 23602766]

Pyz E, Huysamen C, Marshall AS, Gordon S, Taylor PR, and Brown GD (2008). Characterisation of murine MICL (CLEC12A) and evidence for an endogenous ligand. Eur J Immunol 38, 1157–1163. [PubMed: 18350551]

Roesner LM, Ernst M, Chen W, Begemann G, Kienlin P, Raulf MK, Lepenies B, and Werfel T (2019). Human thioredoxin, a damage-associated molecular pattern and Malassezia-crossreactive autoallergen, modulates immune responses via the C-type lectin receptors Dectin-1 and Dectin-2. Sci Rep 9, 11210. [PubMed: 31371767]

Ruprecht K, Kuhlmann T, Seif F, Hummel V, Kruse N, Bruck W, and Rieckmann P (2001). Effects of oncostatin M on human cerebral endothelial cells and expression in inflammatory brain lesions. J Neuropathol Exp Neurol 60, 1087–1098. [PubMed: 11706938]

Sas AR, Carbajal KS, Jerome AD, Menon R, Yoon C, Kalinski AL, Giger RJ, and Segal BM (2020). A new neutrophil subset promotes CNS neuron survival and axon regeneration. Nat Immunol.

Seno A, Maruhashi T, Kaifu T, Yabe R, Fujikado N, Ma G, Ikarashi T, Kakuta S, and Iwakura Y (2015). Exacerbation of experimental autoimmune encephalomyelitis in mice deficient for DCIR, an inhibitory C-type lectin receptor. Exp Anim 64, 109–119. [PubMed: 26176030]

Shan M, Gentile M, Yeiser JR, Walland AC, Bornstein VU, Chen K, He B, Cassis L, Bigas A, Cols M, et al. (2013). Mucus enhances gut homeostasis and oral tolerance by delivering immunoregulatory signals. Science 342, 447–453. [PubMed: 24072822]

Shenderov K, Barber DL, Mayer-Barber KD, Gurcha SS, Jankovic D, Feng CG, Oland S, Hieny S, Caspar P, Yamasaki S, et al. (2013). Cord factor and peptidoglycan recapitulate the Th17-promoting adjuvant activity of mycobacteria through mincle/CARD9 signaling and the inflammasome. J Immunol 190, 5722–5730. [PubMed: 23630357]

Slaets H, Nelissen S, Janssens K, Vidal PM, Lemmens E, Stinissen P, Hendrix S, and Hellings N (2014). Oncostatin M reduces lesion size and promotes functional recovery and neurite outgrowth after spinal cord injury. Mol Neurobiol 50, 1142–1151. [PubMed: 24996996]

Soulika AM, Lee E, McCauley E, Miers L, Bannerman P, and Pleasure D (2009). Initiation and progression of axonopathy in experimental autoimmune encephalomyelitis. J Neurosci 29, 14965–14979. [PubMed: 19940192]

Stanojlovic M, Pang X, Lin Y, Stone S, Cvetanovic M, and Lin W (2016). Inhibition of Vascular Endothelial Growth Factor Receptor 2 Exacerbates Loss of Lower Motor Neurons and Axons

during Experimental Autoimmune Encephalomyelitis. PLoS One 11, e0160158. [PubMed: 27466819]

Steelman AJ, and Li J (2014). Astrocyte galectin-9 potentiates microglial TNF secretion. J Neuroinflammation 11, 144. [PubMed: 25158758]

Steinbach K, Piedavent M, Bauer S, Neumann JT, and Friese MA (2013). Neutrophils amplify autoimmune central nervous system infiltrates by maturing local APCs. J Immunol 191, 4531–4539. [PubMed: 24062488]

Stirling DP, Liu S, Kubes P, and Yong VW (2009). Depletion of Ly6G/Gr-1 leukocytes after spinal cord injury in mice alters wound healing and worsens neurological outcome. J Neurosci 29, 753–764. [PubMed: 19158301]

Stoppelkamp S, Reid DM, Yeoh J, Taylor J, McKenzie EJ, Brown GD, Gordon S, Forrester JV, and Wong SY (2015). Murine pattern recognition receptor dectin-1 is essential in the development of experimental autoimmune uveoretinitis. Mol Immunol 67, 398–406. [PubMed: 26216045]

Taylor PR, Tsoni SV, Willment JA, Dennehy KM, Rosas M, Findon H, Haynes K, Steele C, Botto M, Gordon S, and Brown GD (2007). Dectin-1 is required for beta-glucan recognition and control of fungal infection. Nat Immunol 8, 31–38. [PubMed: 17159984]

Team, R.C. (2013). R: A language and environment for statistical computing. In R Foundation for Statistical Computing.

Thiagarajan PS, Yakubenko VP, Elsori DH, Yadav SP, Willard B, Tan CD, Rodriguez ER, Febbraio M, and Cathcart MK (2013). Vimentin is an endogenous ligand for the pattern recognition receptor Dectin-1. Cardiovasc Res 99, 494–504. [PubMed: 23674515]

Uto T, Fukaya T, Takagi H, Arimura K, Nakamura T, Kojima N, Malissen B, and Sato K (2016). Clec4A4 is a regulatory receptor for dendritic cells that impairs inflammation and T-cell immunity. Nat Commun 7, 11273. [PubMed: 27068492]

Vandenbroeck K, Alvarez J, Swaminathan B, Alloza I, Matesanz F, Urcelay E, Comabella M, Alcina A, Fedetz M, Ortiz MA, et al. (2012). A cytokine gene screen uncovers SOCS1 as genetic risk factor for multiple sclerosis. Genes Immun 13, 21–28. [PubMed: 21716315]

Voskuhl RR, Itoh N, Tassoni A, Matsukawa MA, Ren E, Tse V, Jang E, Suen TT, and Itoh Y (2019). Gene expression in oligodendrocytes during remyelination reveals cholesterol homeostasis as a therapeutic target in multiple sclerosis. Proc Natl Acad Sci U S A 116, 10130–10139. [PubMed: 31040210]

Voskuhl RR, Peterson RS, Song B, Ao Y, Morales LB, Tiwari-Woodruff S, and Sofroniew MV (2009). Reactive astrocytes form scar-like perivascular barriers to leukocytes during adaptive immune inflammation of the CNS. J Neurosci 29, 11511–11522. [PubMed: 19759299]

Wallace PM, MacMaster JF, Rouleau KA, Brown TJ, Loy JK, Donaldson KL, and Wahl AF (1999). Regulation of inflammatory responses by oncostatin M. J Immunol 162, 5547–5555. [PubMed: 10228036]

Wheeler MA, Clark IC, Tjon EC, Li Z, Zandee SEJ, Couturier CP, Watson BR, Scalisi G, Alkwai S, Rothhammer V, et al. (2020). MAFG-driven astrocytes promote CNS inflammation. Nature 578, 593–599. [PubMed: 32051591]

Wheeler MA, and Quintana FJ (2019). Regulation of Astrocyte Functions in Multiple Sclerosis. Cold Spring Harb Perspect Med 9.

Whittaker Hawkins RF, Patenaude A, Dumas A, Jain R, Tesfagiorgis Y, Kerfoot S, Matsui T, Gunzer M, Poubelle PE, Larochelle C, et al. (2017). ICAM1+ neutrophils promote chronic inflammation via ASPRV1 in B cell-dependent autoimmune encephalomyelitis. JCI Insight 2.

Wlodarczyk A, Benmamar-Badel A, Cedile O, Jensen KN, Kramer I, Elsborg NB, and Owens T (2018). CSF1R Stimulation Promotes Increased Neuroprotection by CD11c+ Microglia in EAE. Front Cell Neurosci 12, 523. [PubMed: 30687013]

Wu F, Cao W, Yang Y, and Liu A (2010). Extensive infiltration of neutrophils in the acute phase of experimental autoimmune encephalomyelitis in C57BL/6 mice. Histochemistry and cell biology 133, 313–322. [PubMed: 20063008]

Xu S, Huo J, Lee KG, Kurosaki T, and Lam KP (2009). Phospholipase Cgamma2 is critical for Dectin-1-mediated Ca2+ flux and cytokine production in dendritic cells. J Biol Chem 284, 7038–7046. [PubMed: 19136564]

Ye XC, Hao Q, Ma WJ, Zhao QC, Wang WW, Yin HH, Zhang T, Wang M, Zan K, Yang XX, et al. (2020). Dectin-1/Syk signaling triggers neuroinflammation after ischemic stroke in mice. J Neuroinflammation 17, 17. [PubMed: 31926564]

Yonekawa A, Saijo S, Hoshino Y, Miyake Y, Ishikawa E, Suzukawa M, Inoue H, Tanaka M, Yoneyama M, Oh-Hora M, et al. (2014). Dectin-2 is a direct receptor for mannose-capped lipoarabinomannan of mycobacteria. Immunity 41, 402–413. [PubMed: 25176311]

Yoshida H, Lareau CA, Ramirez RN, Rose SA, Maier B, Wroblewska A, Desland F, Chudnovskiy A, Mortha A, Dominguez C, et al. (2019). The cis-Regulatory Atlas of the Mouse Immune System. Cell 176, 897–912 e820. [PubMed: 30686579]

Young MD, Wakefield MJ, Smyth GK, and Oshlack A (2010). Gene ontology analysis for RNA-seq: accounting for selection bias. Genome Biol 11, R14. [PubMed: 20132535]

Yu G, and He QY (2016). ReactomePA: an R/Bioconductor package for reactome pathway analysis and visualization. Mol Biosyst 12, 477–479. [PubMed: 26661513]

Zhu C, Anderson AC, Schubart A, Xiong H, Imitola J, Khoury SJ, Zheng XX, Strom TB, and Kuchroo VK (2005). The Tim-3 ligand galectin-9 negatively regulates T helper type 1 immunity. Nat Immunol 6, 1245–1252. [PubMed: 16286920]

HIGHLIGHTS

- Dectin-1 limits experimental autoimmune encephalomyelitis (EAE)
- Dectin-1 upregulates *Osm* in myeloid cells via a Card9-independent pathway
- OsmR signaling in astrocytes limits EAE severity
- Galectin-9 is an endogenous ligand of Dectin-1 made by astrocytes and limits EAE

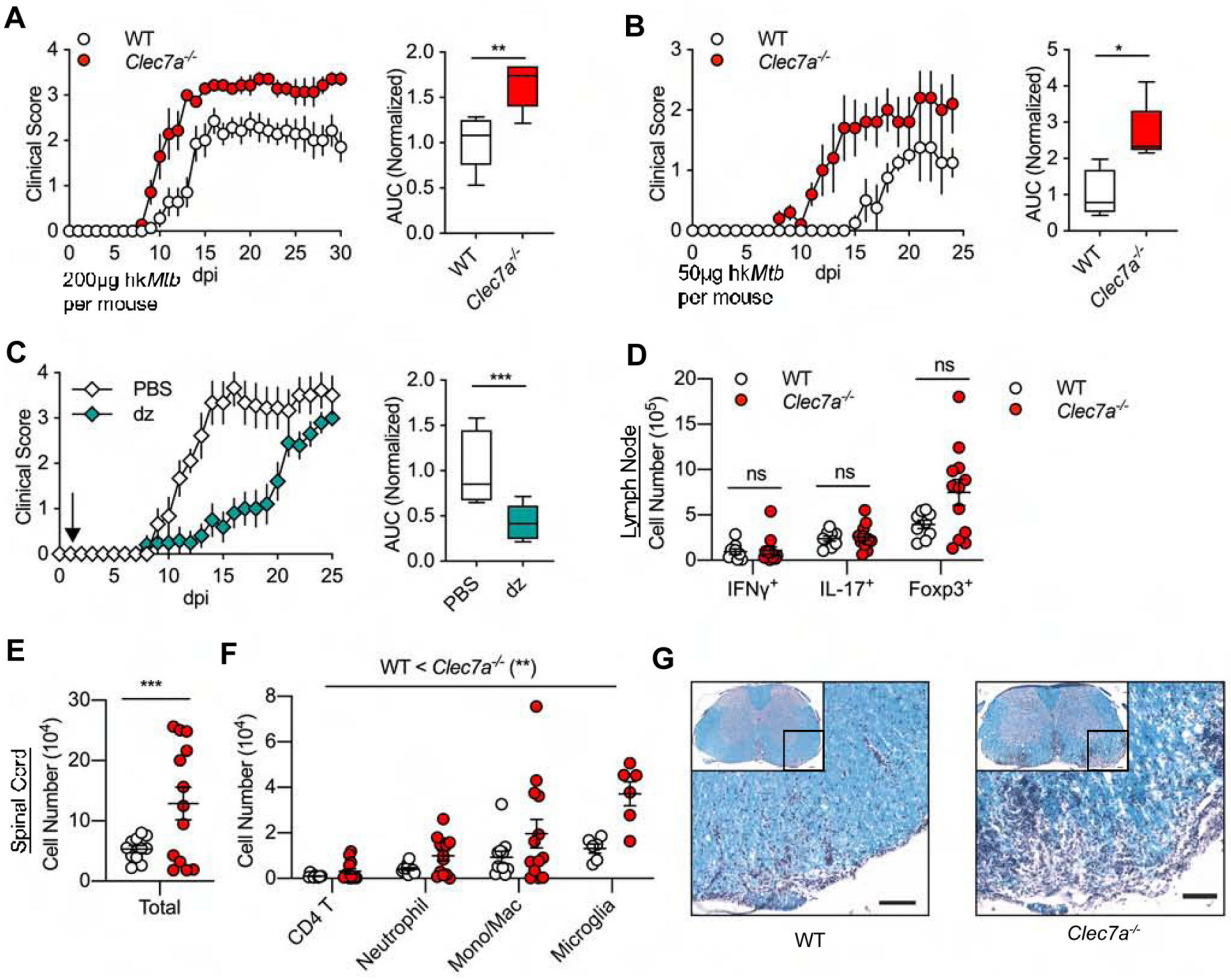

Figure 1. Dectin-1 limits neuroinflammation in EAE.

(A-C) EAE clinical scores (left panels) and AUC (right panels) for statistical analysis. Comparison between WT and *Clec7a*$^{-/-}$ mice using standard immunization (200 µg hk*Mtb*/mouse) with n=7 mice/group (A) or reduced adjuvant immunization (50 µg hk*Mtb*/mouse) with n=4 WT and n=5 *Clec7a*$^{-/-}$ mice/group (B). Comparison of WT mice receiving either hot alkali-depleted zymosan (dz) (500µg/mouse)(n=10) or PBS (n=9) *i.v.* at 1-dpi with standard immunization (C). Data representative of >3 independent experiments (A) or 2 independent experiments each (B, C). **(D)** Numbers of Th cell subsets in ILN between WT and *Clec7a*$^{-/-}$ mice at 9-dpi. Data representative of 3 independent experiments. **(E, F)** Total cell numbers (E) and numbers of indicated cell types **(F)** in spinal cord at 9-dpi. The main effect of genotype (WT < *Clec7a*$^{-/-}$) (**) by 2-factor RM-ANOVA indicated in (F). Data are combined from three independent experiments. One datapoint denotes a result from one mouse (D-F). **(G)** LFB-PAS staining of lumbar SC in WT and *Clec7a*$^{-/-}$ mice at EAE 17-dpi. Scale 100 µm. Representative images from 10 mice/group combined from two independent experiments. Please also see Figures S1, 2.

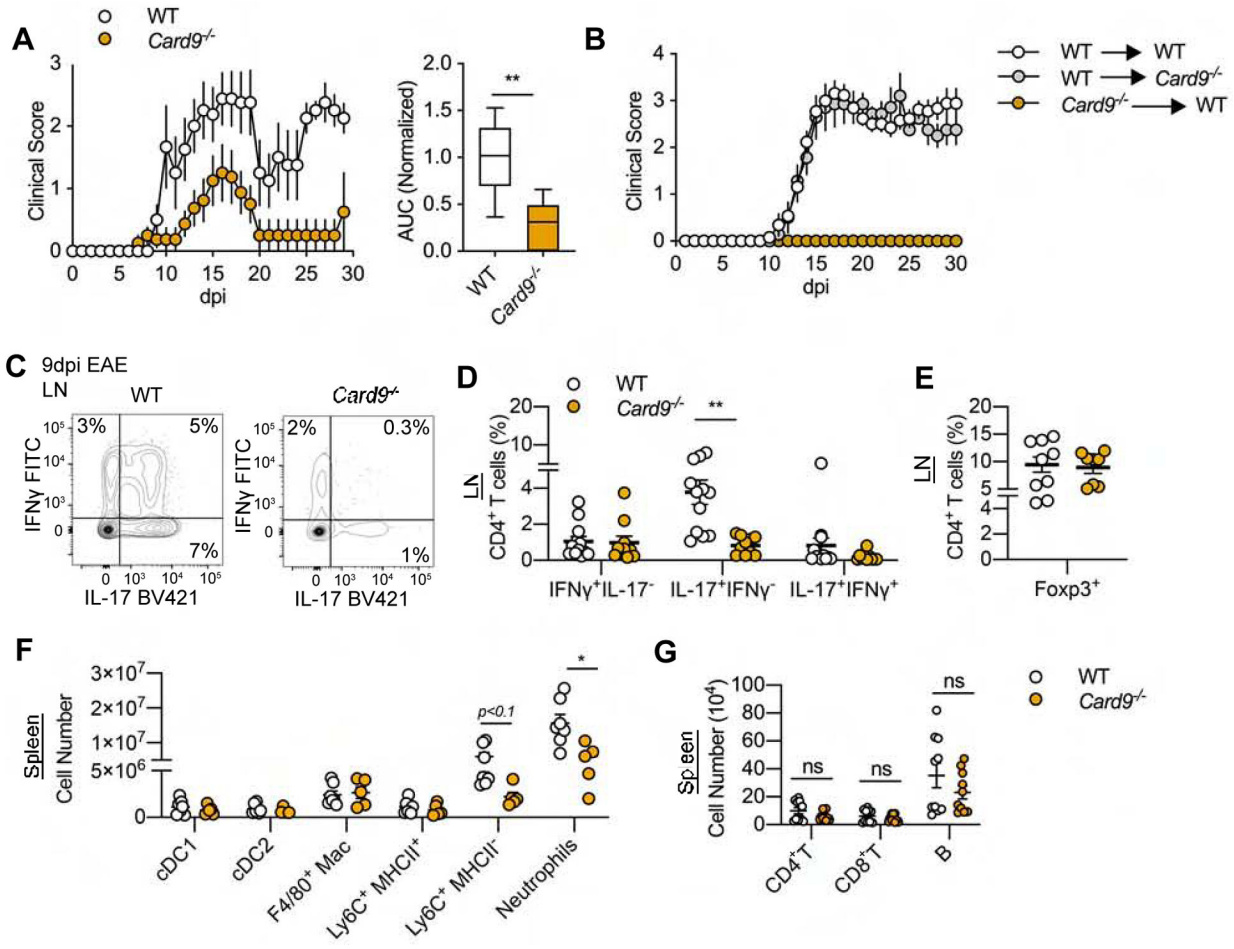

Figure 2. Card9 exacerbates EAE and promotes a Th17 response.

(A) EAE clinical scores (left panel) and AUC (right panel) for statistical analysis. Comparison between WT (n=9) and *Card9*$^{-/-}$ (n=8) mice. Data are combined from two independent experiments. **(B)** EAE clinical scores from BM chimeras. WT BM cells were transferred to irradiated WT (white) or *Card9*$^{-/-}$(gray) recipients. Another group is *Card9*$^{-/-}$ BM transferred to WT recipients (orange). n=7–13 mice/group, combined from three independent experiments. **(C-G)** Leukocytes in peripheral lymphoid organs at 9-dpi EAE. Representative flow cytometry plots for intracellular cytokine staining (C) and frequency of Th cell subsets in ILN (D, E). Numbers of indicated cell types in spleen (F, G). One datapoint denotes a result from one mouse. Data are combined from three independent experiments. Please also see Figure S3.

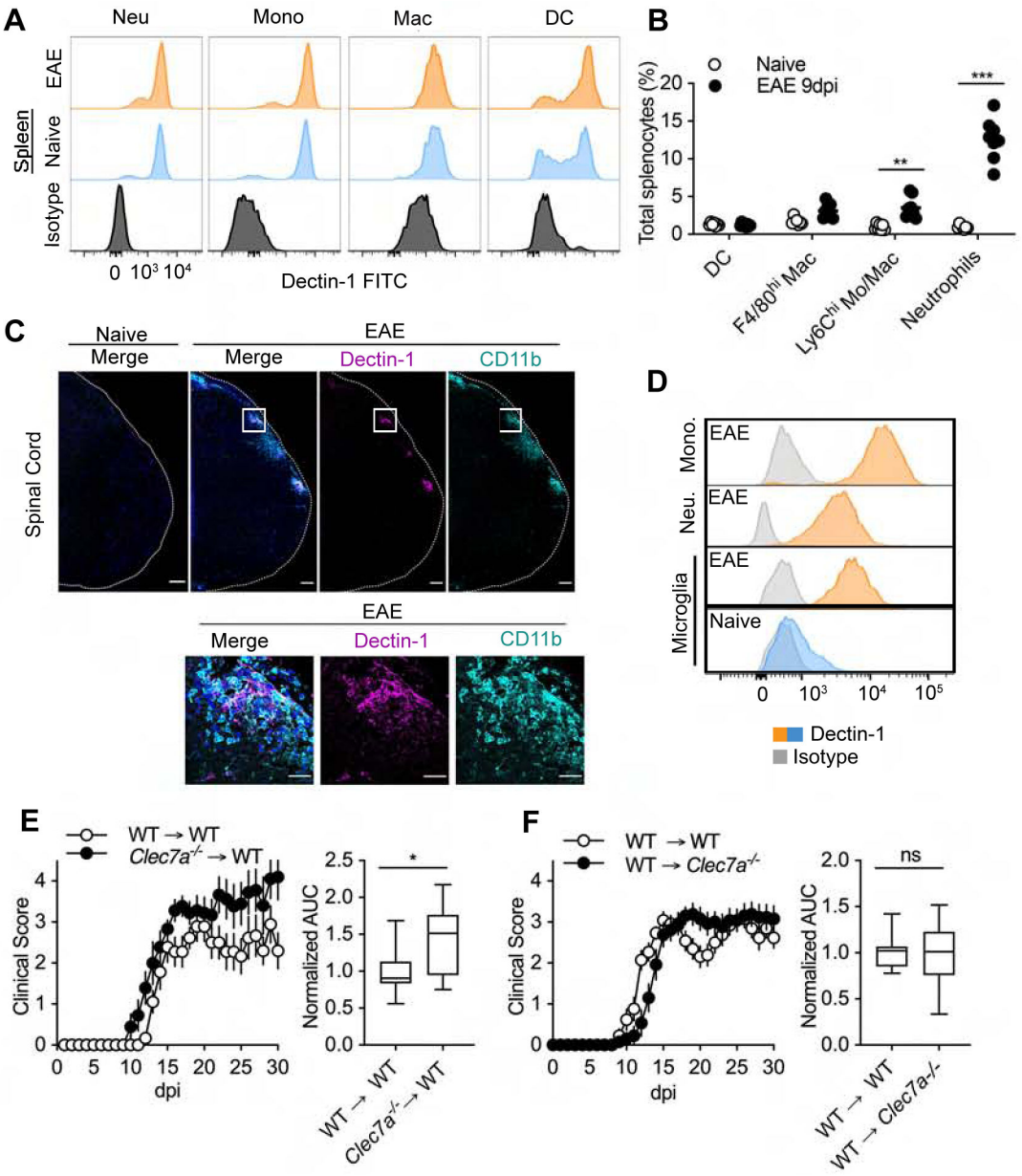

Figure 3. Cell type-specific Dectin-1 expression and function.

(A) Flow cytometry histograms, indicating Dectin-1 expression in splenic neutrophils ($CD11b^{+}Ly6G^{+}$), monocytes ($CD11b^{+}Ly6C^{+}Ly6G^{-}$), macrophages ($CD11b^{+}F4/80^{hi}$), and DCs ($CD11b^{+}CD11c^{+}$) from naïve and EAE 9-dpi WT mice. **(B)** Frequency of myeloid cell subsets in total splenocytes in naïve (n=7) and EAE 9-dpi (n=8) mice. Data are combined from 2 independent experiments. **(C)** Localization of Dectin-1 expressing cells with CD11b counter-staining in the lumbar SC of naïve and EAE 17-dpi mice. Bottom panels are enlarged images of regions indicated with squares in top panels. Scale 100 μm in upper panels and 25 μm in lower panels. **(D)** Flow cytometry histograms of Dectin-1 expression in microglia ($CD11b^{lo}CD45^{lo}Tmem119^{+}$), neutrophils ($CD11b^{+}Ly6G^{+}$), and monocytes ($CD11b^{+}Ly6G^{-}Ly6C^{+}$) in SC from naïve and EAE 16-dpi mice. Representative data from

two independent experiments. **(E, F)** EAE scores (left panels) and AUC for statistical analysis (right panels) of irradiation BM chimeras. WT or *Clec7a*$^{-/-}$ BM cells into irradiated WT recipients (n=9 for both groups) (E). WT BM into WT or *Clec7a*$^{-/-}$ recipients using (n=13 for both groups) (F). Data are combined from two independent experiments each. Please also see Figure S4.

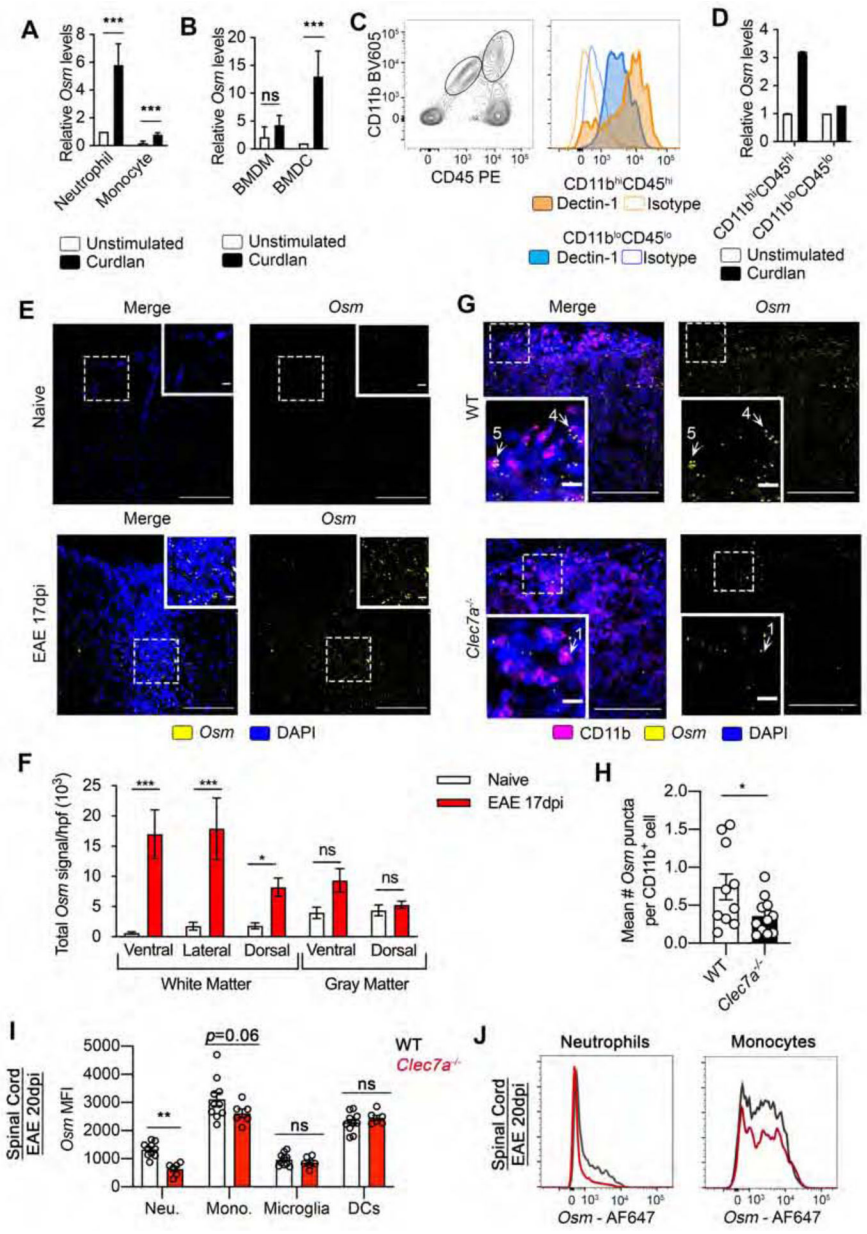

Figure 4. Dectin-1 promotes expression of Oncostatin M (Osm).

(A, B) *Osm* mRNA expression in indicated myeloid cell types with *ex vivo* curdlan (100 μg/ml) stimulation for 3 hrs. Evaluated are flow-cytometry sorted BM monocytes (CD11b $^{+}$Ly6C^{hi}Ly6G^{-}) and neutrophils (CD11b^{+}Ly6G^{+}) (A), as well as GM-CSF-derived BMDCs and M-CSF-derived BMDM (B). Post-hoc Sidak test following 2-factor ANOVA indicated in (A, B). Mean ± SEM shown. Data are combined from two independent experiments. **(C, D)** Analyses of myeloid cells from SC and brain of EAE mice at 30-dpi. Gating of CD11b^{lo}CD45^{lo} and CD11b^{hi}CD45^{hi} cells from and evaluation for Dectin-1 expression by flow cytometry (C). Gated cells in (C) were flow cytometry sorted, stimulated with curdlan (100μg/ml) for 3 hr *ex vivo*, and amounts of *Osm* mRNA were evaluated by RT-qPCR (D). Samples pooled from 2 mice each. Representative of 2 independent experiments. **(E)**

Representative images from two independent experiments of RNAscope *in situ* hybridization (ISH) of *Osm* mRNA in the lumbar SC of WT naïve and EAE 17-dpi mice. Scale bars, 100 μm in main panels, 10 μm in inset. **(F)** Region-specific quantification of *Osm* mRNA signal per hpf (sum of integrated density) in lumbar SC regions from WT naïve and EAE 17-dpi mice using n=4 mice/group, analyzed by 2-factor ANOVA of log-transformed data with post-hoc Sidak test shown. Representative of two independent experiments. **(G)** Representative images from two independent experiments of combined ISH of *Osm* mRNA and CD11b staining in the ventrolateral white matter of lumbar SC from WT and *Clec7a*$^{-/-}$ mice at 17-dpi EAE. Scale bars, 100 μm in main panels, 10 μm in inset. **(H)** Quantification of mean *Osm* mRNA puncta per CD11b^{+} cell. One datapoint denotes a result from one mouse. Mean ± SEM. Data from two independent experiments. **(I, J)** Evaluation of *Osm* mRNA expression in CNS myeloid cell subsets at 20-dpi EAE by PrimeFlow. Quantification of *Osm* MFI (I) and representative histograms of *Osm* expression (J). One datapoint denotes a result from one mouse. Data from two independent experiments. Please also see Figure S4.

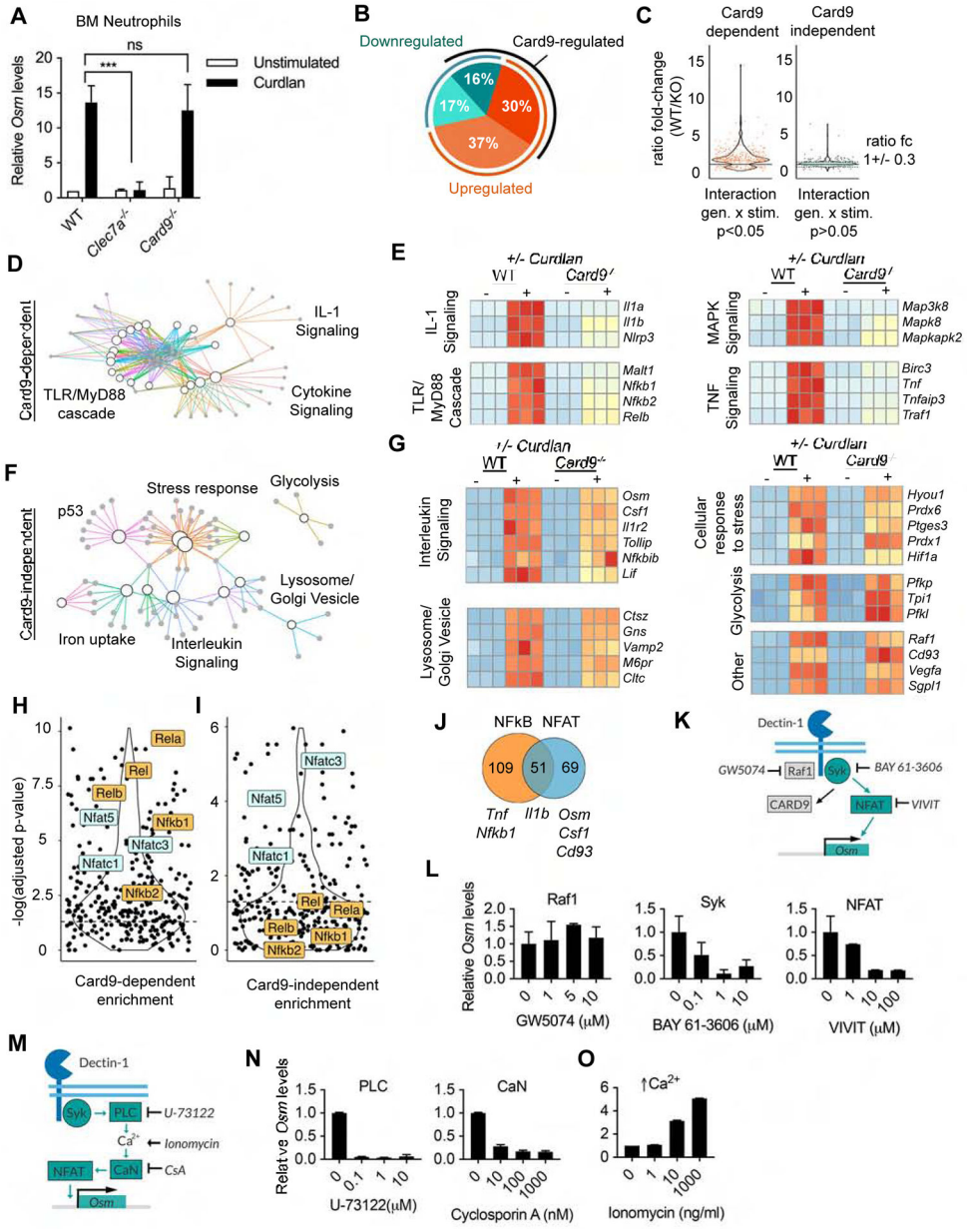

Figure 5. Defining the Card9-independent Dectin-1 transcriptional program.

(A) *Osm* mRNA expression in BM neutrophils from WT, *Clec7a*$^{-/-}$, and *Card9*$^{-/-}$ mice. Neutrophils were treated with or without curdlan (100 μg/ml) *ex vivo* for 3 hrs. Mean ± SEM, *n*=3 mice/group. Representative of 3 independent experiments. **(B-G)** RNAseq analyses of BM neutrophils from WT and *Card9*$^{-/-}$ mice (*n*=3 mice/group) treated with or without curdlan (100 μg/ml) *ex vivo* for 3 hrs. Proportions of genes which are up- or down-regulated in a Card9-dependent manner, in WT neutrophils with curdlan stimulation (B). Ratio of gene expression fold-change, comparing WT and *Card9*$^{-/-}$ (KO) neutrophils, with curdlan stimulation (points indicate individual genes) (C). Gene-concept network based on RNAseq results, showing pathway enrichment analysis (D, F). Heatmaps of selected genes with indicated associated pathways (E, G). Card9-dependent and -independent candidate

genes are indicated in (D, E) and (F, G), respectively. **(H, I)** Plots of adjusted p-values for TF binding site enrichment near Card9-dependent genes (H) or Card9-independent genes (I). NFAT family and NFκB family TFs are indicated in turquoise and orange, respectively. **(J)** Venn diagram of genes with at least 3 predicted NFκB or NFAT binding sites in OCRs within 100 kb of each gene. **(K)** Schematic of Dectin-1 signaling with small molecule inhibitors. **(L)** RT-qPCR evaluation of *Osm* mRNA in WT BM neutrophils pre-treated with inhibitors at the indicated doses for 1 hr before curdlan stimulation (100 μg/ml) for 3 hrs. Data representative of 2 independent experiments. **(M)** Schematic of small molecule targets. **(N, O)** *Osm* mRNA in WT BM neutrophils stimulated with curdlan (100 μg/ml) for 3hrs after 1 hr pretreatment indicated small molecules (N), or with ionomycin (O). Data representative of two independent experiments (L, N, O). Please also see Figure S5.

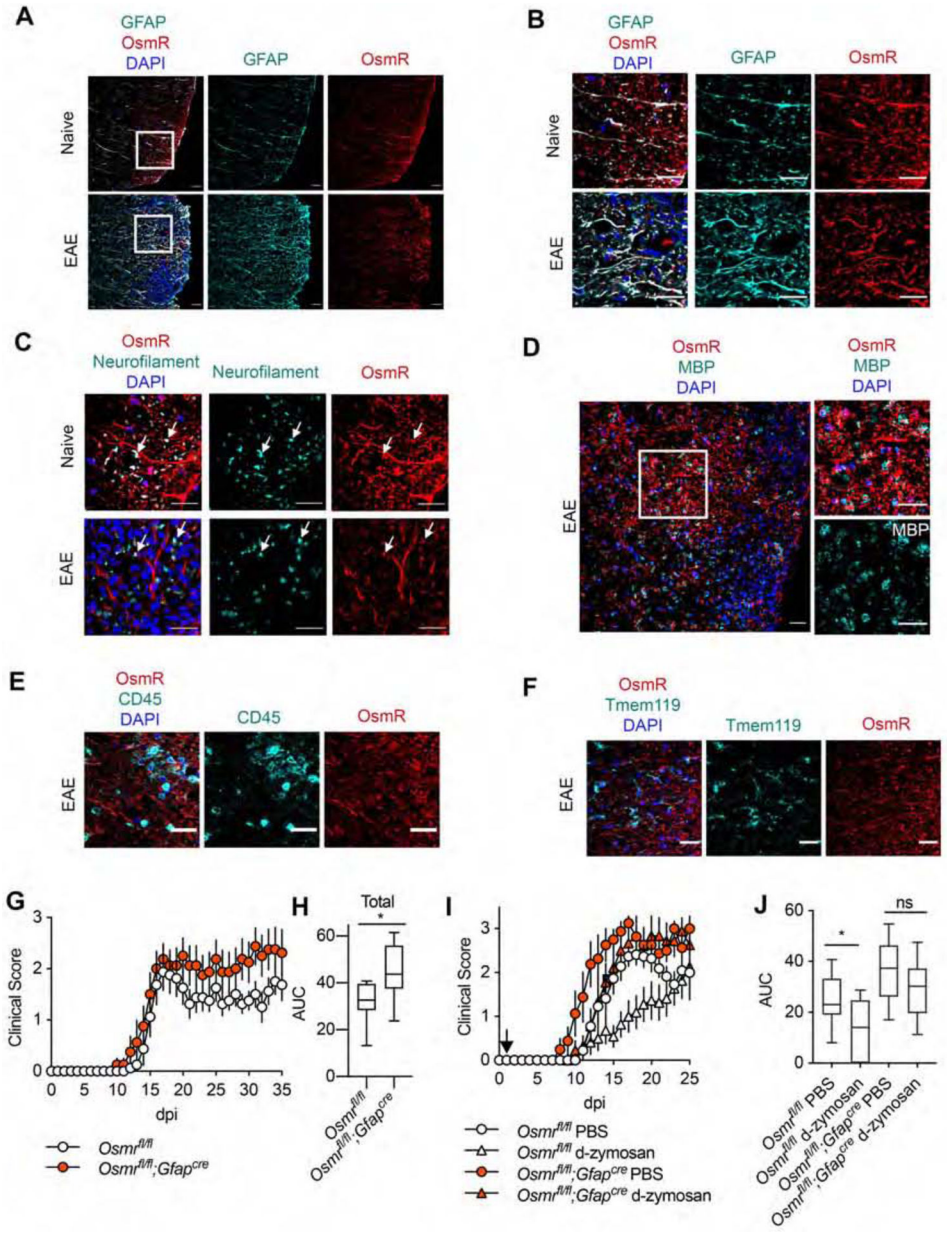

Figure 6. OsmR expression in astrocytes limits EAE severity.

(A-F) OsmR expression in ventro-lateral white matter of lumbar SC from naïve and EAE 17-dpi mice along with counter-staining for GFAP (A, inset in B), Neurofilament (C), MBP (D), CD45 (E), or Tmem119 (F). Scale bar, 25μm. Representative images from two independent experiments (total n=5 mice/group). **(G, H)** EAE scores of *Osmr*$^{fl/fl}$ and *Osmr*$^{fl/fl}$*;Gfap*^{cre} littermates (n=8 mice/group). Data quantified by total AUC (H). Representative of 3 independent experiments. **(I, J)** EAE scores of *Osmr*$^{fl/fl}$ and *Osmr*$^{fl/fl}$*;Gfap*^{cre} littermates (n=8–11 mice/group) administered PBS or d-zymosan *i.v.* at 1-dpi EAE. Data quantified by total AUC (J). Data combined from 2 independent experiments. Please also see Figure S6.

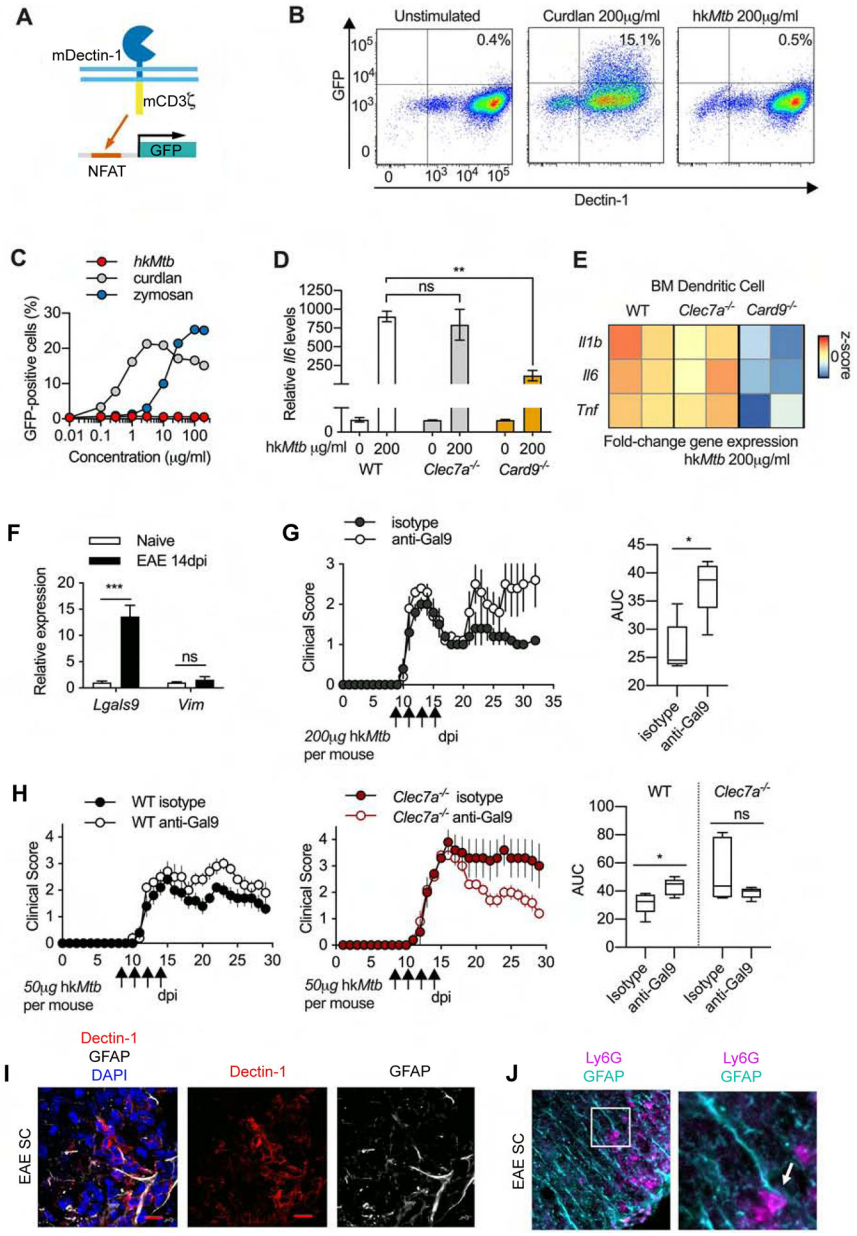

Figure 7. Dectin-1 responds to Gal-9 but not to hk*Mtb*, EAE adjuvant.

(A) Schematic of the Dectin-1 stimulation reporter cell line. Extracellular and trans-membrane domains of mouse Dectin-1 were fused to the cytoplasmic domain of CD3ζ. Activation of Dectin-1 was detected by a GFP reporter. **(B)** Representative flow cytometry results from two independent experiments, showing Dectin-1-GFP reporter at 20-hrs with or without curdlan (200 μg/ml) or hk*Mtb* (200 μg/ml) stimulation in tissue culture. Values indicate percentages of $GFP^+Dectin\text{-}1^+$ cells. **(C)** Proportions of $GFP^+Dectin1^+$ mDectin-1/mCD3ζ-GFP reporter cells with titrated concentrations of hk*Mtb*, zymosan, or curdlan with indicated concentrations. **(D, E)** RT-qPCR analysis of *Il6* normalized to unstimulated control (D) and heatmap of *Il1b, Il6*, and *Tnf* expression normalized to unstimulated control (E). WT, *Clec7a*$^{-/-}$, and *Card9*$^{-/-}$ BMDCs stimulated with 200 μg/ml hk*Mtb* in tissue culture for

3 hrs. Mean ± SEM of duplicate wells shown, with data representative of two independent experiments. **(F)** *Lgals9* and *Vim* mRNA in total SC homogenates from naïve and EAE 14-dpi WT mice. Mean ± SEM, n=3 mice/group. **(G)** EAE scores of WT mice administered anti-Gal9 antibody or isotype control intrathecally on day 9, 11, 13, 15. n=5 mice/group), quantified by AUC (right panel). **(H)** EAE scores of WT mice and *Clec7a*$^{-/-}$ mice administered anti-Gal9 antibody or isotype control intrathecally on day 9, 11, 13, 15. Mean ± SEM shown, n=5 mice/group. Data quantified by AUC (right panel). **(I, J)** Representative images from two independent experiments of astrocytes vs. Dectin-1-expressing cells (I) or neutrophils (J). Samples were obtained from SC of WT mice at 17-dpi EAE. Please also see Figure S7.

KEY RESOURCES TABLE

REAGENT or RESOURCE	SOURCE	IDENTIFIER
Abs		
Rat monoclonal anti-CD3e (clone 145–2C11)	BioLegend	Cat# 100306
Rat monoclonal anti-CD4 (clone GK1.5)	BioLegend	Cat# 100451
Armenian hamster anti-TCR-β (clone H57–597)	BioLegend	Cat# 109221
Rat monoclonal anti-CD25 (clone PC61)	BioLegend	Cat# 102003
Rat monoclonal anti-CD8 (clone 53–6.7)	BioLegend	Cat# 100722
Rat monoclonal anti-IFNy (clone XMG1.2)	BioLegend	Cat# 505806
Rat monoclonal anti-IL-17 (clone TC11–18H10.1)	BioLegend	Cat# 506904
Rat IgG1, κ isotype control (clone RTK2071)	BioLegend	Cat# 400429
Rat monoclonal anti-Foxp3 (clone MF-14)	BioLegend	Cat# 126405
Rat monoclonal anti-GM-CSF (clone MP1–22E9)	BioLegend	Cat# 505405
Rat IgG2a, κ isotype control (clone RTK2758)	BioLegend	Cat# 400507
Rat monoclonal anti-CD45 (clone 30-F11)	BioLegend	Cat# 103114
Rat monoclonal anti-CD45 (clone 30-F11)	BD	Cat# 564279
Rat monoclonal anti-CD11b (clone M1/70)	BioLegend	Cat# 101257
Rat monoclonal anti-CD11c (clone N418)	BioLegend	Cat# 117310
Rat monoclonal anti-Ly6G (clone 1A8)	BioLegend	Cat# 127606
Rat monoclonal anti-Ly6C (clone HK1.4)	BioLegend	Cat# 128008
Rat monoclonal anti-CD19 (clone 6D5)	BioLegend	Cat# 115530
Rat monoclonal anti-IA/IE (clone M5/114.15.2)	BioLegend	Cat# 107622
Rat monoclonal anti-CD40 (clone 3/23)	BioLegend	Cat# 124609
Rat monoclonal anti-CD80 (clone 16–10A1)	BioLegend	Cat# 104733
Rat monoclonal anti-CD86 (clone GL-1)	BioLegend	Cat# 105018
Rat monoclonal anti-F4/80 (clone BM8)	BioLegend	Cat# 123114
Rat monoclonal anti-Dectin-1 (clone 2A11)	Biorad	Cat# MCA2289FA
Rat IgG2b isotype control (clone RTK4530)	BioLegend	Cat# 400606
Rat monoclonal anti-Tmem119 (clone 106–6)	Abcam	Cat# ab210405
Goat polyclonal anti-Rabbit (H+L) Highly Cross-Adsorbed Secondary Ab	ThermoFisher	Cat# 21245
Rat monoclonal anti-CD45.1 (clone A20)	BioLegend	Cat# 110708
Rat monoclonal anti-CD45.2 (clone 104)	BioLegend	Cat# 109814
Rat monoclonal anti-CD11b (clone EPR19387)	Abcam	Cat# ab184308
Rat monoclonal anti-Tmem119 (clone 28–3)	Abcam	Cat# ab209064
Goat polyclonal anti-Iba1	Novus	Cat# NB100–1028
Rat monoclonal anti-OsmR (clone 18125)	R&D	Cat# MAB662
Rat IgG2a isotype control (clone RTK2758)	BioLegend	Cat# 400501
Rabbit polyclonal anti-GFAP	Abcam	Cat# ab7260
Mouse monoclonal anti-GFAP (clone 5C10)	Novus	Cat# 05197

REAGENT or RESOURCE	SOURCE	IDENTIFIER
Rat monoclonal anti-CD45 (clone 30-F11)	BioLegend	Cat# 103104
Rabbit polyclonal anti-MBP	Abcam	Cat# ab40390
Rabbit polyclonal anti-Neurofilament heavy	Abcam	Cat# ab8135
Chicken polyclonal anti-Rat IgG (H+L) Cross-Adsorbed Secondary Ab	ThermoFisher	Cat# A-21472
Goat polyclonal anti-Mouse IgG (H+L) Cross-Adsorbed Secondary Ab	ThermoFisher	Cat# A-11029
Donkey polyclonal anti-Rabbit (H+L) Highly Cross-Adsorbed Secondary Ab	ThermoFisher	Cat# A-21206
Donkey polyclonal anti-Goat (H+L) Highly Cross-Adsorbed Secondary Ab	ThermoFisher	Cat# A-11055
Goat polyclonal anti-Rabbit (H+L) Highly Cross-Adsorbed Secondary Ab	ThermoFisher	Cat# A-21244
Bacterial and Virus Strains		
retroviral pMXs-IP-mCD3ζ-mDectin1 vector	gift from Gordon Brown (University of Aberdeen, UK) (under MTA)	N/A
Biological Samples		
N/A		
Chemicals, Peptides, and Recombinant Proteins		
Curdlan (from *Alcaligenes faecalis*, beta-1,3 Glucan hydrate)	Sigma-Aldrich	Cat# C7821
Zymosan Depleted (hot-alkali treated zymosan)	InvivoGen	Cat# tlr-zyd
GW5074 (Raf1 inhibitor)	Sigma-Aldrich	Cat# G6416
BAY 61-36-6 (Syk inhibitor)	Cayman Chemical	Cat# 11423
NFAT Inhibitor (11R-VIVIT)	Cayman Chemical	Cat# 13855
Cyclosporine A (Calcineurin inhibitor)	Cayman Chemical	Cat#12088
U-73122 (Phospholipase C inhibitor)	Cayman Chemical	Cat# 70740
Recombinant mouse GM-CSF	BioLegend	Cat# 576304
Recombinant mouse M-CSF	BioLegend	Cat# 576406
Dynabeads Mouse T-activator CD3/CD28	Gibco	Cat# 11456D
$MOG_{35–55}$ peptide (MEVGWYRSPFSRVVHLYRNGK)	United Biosystems	Cat# U104628
Freund's adjuvant, complete (contains *Mycobacterium tuberculosis* (H37Ra, ATCC 25177), heat killed and dried)	Sigma-Aldrich	Cat# F5881
Freund's adjuvant, incomplete (does not contain *Mycobacteria tuberculosis*)	Sigma-Aldrich	Cat# F5506
Pertussis Toxin	List Biological Technologies	Cat# 180
LFB Solvent Blue 38	Sigma-Aldrich	Cat# S3382
Gill's Hematoxylin No. 3 for tissue	Sigma-Aldrich	Cat# GHS316
Schiff's reagent	Sigma-Aldrich	Cat# S5133
Collagenase D (from *Clostridium histolyticum*)	Roche	Cat# 11088866001
Ionomycin (calcium salt from *Streptomyces conglobatus*)	Sigma-Aldrich	Cat# I0634
Phorbol 12-myristate 13-acetate (PMA)	Sigma-Aldrich	Cat# P 1585
Prolong Gold Antifade Mountant	Thermo-Fischer	Cat# P36930
Mycobacterium tuberculosis H37 Ra, Desiccated (Heat-killed *Mtb*)	BD Difco	Cat# 231141

REAGENT or RESOURCE	SOURCE	IDENTIFIER
RNAscope Probe- Mm-Osm	ACD	Cat# 427071
PrimeFlow RNA Assay Probe- Mm-Osm	Invitrogen	Cat# VB1–10808-PF
Critical Commercial Assays		
Cytofix/Cytoperm Kit	BD	Cat# 554714
FOXP3 Fix/Perm Kit	BioLegend	Cat# 421401
CellTrace Violet Cell Proliferation Kit	Invitrogen	Cat# C34557
LIVE/DEAD Fixable Violet Dead Cell Stain Kit	Thermo-Fisher	Cat# L34955
Mouse Oncostatin M/OSM DuoSet ELISA Kit	Fischer (R&D Systems)	Cat# DY49505
EasySep Mouse CD4+ T Cell Isolation Kit	StemCell Technologies	Cat# 19852
Mouse IL-10 ELISA MAX Assay	BioLegend	Cat# 431411
PrimeFlow RNA Assay Kit	Invitrogen	Cat# 88-18005-204
Deposited Data		
Raw and analyzed RNA-seq data for “Genome-wide analysis of the CARD9/Dectin-1 transcriptional program in neutrophils and macrophages by RNA-seq”	This paper	GSE148850
Analyzed microarray data for “Gene expression profiling of multiple sclerosis pathology identifies early patterns of demyelination surrounding chronic active lesions”	Hendrickx et al, 2017	GSE108000
Analyzed RNA-seq data for “Human brain tissues from healthy controls and multiple sclerosis patients”	Voskuhl et al, 2019	GSE123496
Mouse reference genome, version GRCm38v73	Genome Reference Consortium	https://www.ncbi.nlm.nih.gov/grc/mouse
Analyzed ATAC-seq data for BM neutrophils (GN_BM) and monocytes (Mo_6C+II-_Bl)	Yoshida et al, 2019; Immunological Genome Project (Heng et al, 2008)	http://rstats.immgen.org/Chromatin/chromatin.html
Analyzed RNA-seq data for *Osmr* expression	Immunological Genome Project (Heng et al, 2008)	http://rstats.immgen.org/Skyline/skyline.html
Experimental Models: Cell Lines		
Mouse: 58$\alpha^-\beta^-$ T hybridoma cell line with stable expression of a NFAT-GFP-hCD4 RV reporter construct	From laboratory of Ken Murphy (Washington University, USA) (Ise et al, 2010)	N/A
Human: BOSC-23 cells, retrovirus packaging cell line	N/A	RRID:
Experimental Models: Organisms/Strains		
Mouse: *Clec7a*$^{-/-}$;B6.*Clec7a*^{tm1Gdb}/*J*	Generated by the laboratory Dr. Gordon Brown (University of Aberdeen, UK) (Taylor et al, 2007)	N/A
Mouse: *Card9*$^{-/-}$ (C57BL/6)	Generated by the laboratory Dr. Xin Lin (M.D. Anderson Cancer Center, Houston, TX) (Hsu et al, 2007)	N/A
Mouse: *Osmr*$^{fl/fl}$; B6;129-*Osmr*$^{tm1.1Nat}$/J (Backcrossed to the C57BL/6 background for this paper)	The Jackson Laboratory	JAX #011081
Mouse: *Aldh1l1-eGFP;* Tg(Aldh1l1-EGFP)OFC789Gsat/Mmucd	Generated by the laboratory of Dr. Ben Barres (Stanford University, USA) (Cahoy et al, 2008)	RRID:MMRRCC_001015-UCD

REAGENT or RESOURCE	SOURCE	IDENTIFIER
Mouse: *Gfap*^{cre}; B6.Cg-Tg(Gfap-cre)77.6Mvs/2J	The Jackson Laboratory	JAX #024098
Oligonucleotides		
Primers for RT-qPCR: see Table S1	This paper	N/A
Primers for *Osmr*$^{fl/fl}$ recombination: see Table S1	This paper	N/A
Recombinant DNA		
pMXs-IP-mCD3ζ-Dectin-1	Gift from Dr. Gordon Brown (University of Aberdeen, UK) (Under MTA) (Pyz et al, 2010)	N/A
Software and Algorithms		
R statistical programming environment	Team et al, 2013	https://www.r-project.org
Bioconductor	Huber et al, 2015	https://bioconductor.org
DESeq2	Love et al, 2014	https://bioconductor.org/packages/release/bioc/html/DESeq2.html
Cutadapt	Martin et al, 2011	https://github.com/marcelm/cutadapt/
STAR	Dobin et al, 2013	https://github.com/alexdobin/STAR
ReactomePA	Yu et al, 2016	http://bioconductor.org/packages/release/bioc/html/ReactomePA.html
GOseq	Young et al, 2010	https://bioconductor.org/packages/release/bioc/html/goseq.html
ImageJ	Schindelin et al., 2012	https://imagej.net/Fiji
FlowJo	N/A	https://www.flowjo.com/solutions/flowjo
GraphPad Prism	N/A	https://www.graphpad.com/scientific-software/prism/
Other		
Documentation: analysis of Card9-dependent and -independent gene sets, transcription factor enrichment	This paper	https://github.com/medeerhake/manuscript_03